東京大学 大学院新領域創成科学研究科
基盤科学研究系
先端エネルギー工学専攻

平成 23 年度

修士論文

Analytical Study of Reed Valve Air-breathing System for Microwave Rocket

－マイクロ波ロケットのためのリード弁を用いた空気吸い込み機構の解析－

2012 年 2 月提出
指導教員　小紫　公也　教授

47106067　福成　雅史

Contents

List of Figure

Chapter 1

Introduction: Microwave Rocket and Microwave Source Concept

1.1 Background of Microwave Rocket

A lot of space exploration and development plans such as the Solar Power Satellite or Space Factory have been proposed. These plans can contribute to human's life and society, and have important meanings for science. However they need huge amount of cost to achieve. One of the biggest costs is the cost of mass transportation to the space, because launch cost using a conventional chemical rocket reaches about 1 million yen per 1 kg payload. A chemical rocket requires huge fuel to get sufficiently velocity; therefore, its payload ratio is only several percent. This is reason why the cost becomes huge. In addition the chemical rocket needs complex and expensive components such as a turbo pump. These complex components make manufacturing cost high and operation during flight difficult.

In order to solve the problems, new launching system is requierd. Beamed energy propulsion (BEP) is one of the most promising candidates for a future low-cost launch system. Figure1-1 shows schematic of BEP launching. The concept of BEP was suggested by Arthur Kantrowitz using laser launch system in 1972 [1]. BEP system gains propulsive energy by a high-power beamed electromagnetic wave radiated from the ground or a space-based facility. Since BEP vehicle do not require an on-board energy source, pumping system or atomic reactors, the structure of BEP is very simple and manufacturing cost can be reduced. Additionally BEP vehicle uses ambient air as propellant during its atmospheric flight, so that the specific impulse I_{sp} and payload ratio could be much high than chemical rockets.

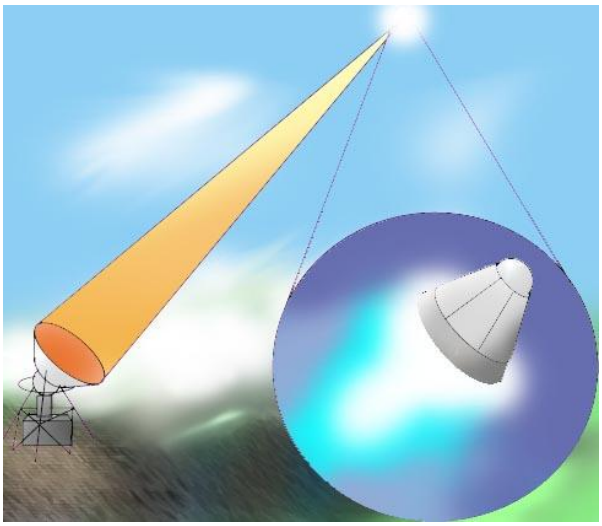

Figure 1-1 Schematic figure of Beamed Energy Propulsion

Various approaches to laser propulsion and laser launch ware explored. A remarkable result is a launch demonstration conducted by Myrabo *et al*. achieving 71m launching [2]. On the other hand, for BEP using microwave, Knecht conducted an analysis on microwave thermal rocket system which propellant is heated by microwave, in 1980s [3]. Batanov also conducted analysis using microwave which beam width is 10mm [4]. Our research group also investigates microwave propulsion called as "Microwave Rocket" [5-7]. Microwave has some advantages compare with laser. Microwave generator is being developed in field of nuclear fusion as heat source of core plasma and has already realized 1MW class beam power [8] and high energy conversion efficiency. Furthermore its cost per beam power is 2order smaller than that of laser.

For these reasons, we propose Microwave rocket as the most promising idea to make it easy to exploration to the space.

1.2 Microwave source and its Feasibility for Application to Microwave Rocket

Figure 1-2 shows schematic outline of the gyrotron. Gyrotron is a powerful microwave generator using a principle of Electron Cyclotron Maser (ECM). As shown in Fig.1-2, gyrotron consists electron gun called Magnetron Injection Gun (MIG), beam tunnel, cavity resonator, mode converter collector and output window. External magnetic field needed for oscillation is generated by Super Conducting Magnet (SCM). Circling electron beam radiated from MIG guided by external magnetic field, is accelerated in a circling direction and enters the cavity. In the cavity, the beam interacts with TE microwave and the some of the energy of the electron beam is converted into microwave power. After the energy converting, the electron beam is captured by collector and leftover kinetic energy converts to thermal energy meanwhile microwave oscillated in the cavity radiates from output window through waveguides and collector [9].

Gyrotron is developed for mainly plasma start-up and electron cyclotron resonance heating (ECRH) in tokamaks and stellarators , as well as non-inductive current drive and stability control in tokamak plasma[10]. However, gyrotoron has a wide range of application including radars, atmospheric sensing, advanced communication materials processing and extra-high-resolution spectroscopy, etc [11]. Microwave rocket is one of the applications of Gyrotron. A 1MW-class gyrotron developed by Japan Atomic Energy Agency (JAEA) is hown in Fig.1-3 is used for microwave rocket experiments in our laboratory.

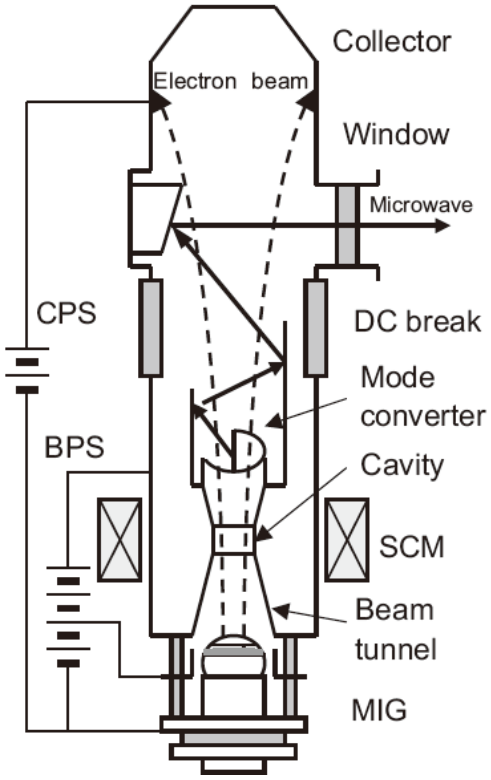

Figure1-2 Schematic of Gyrotron[9]

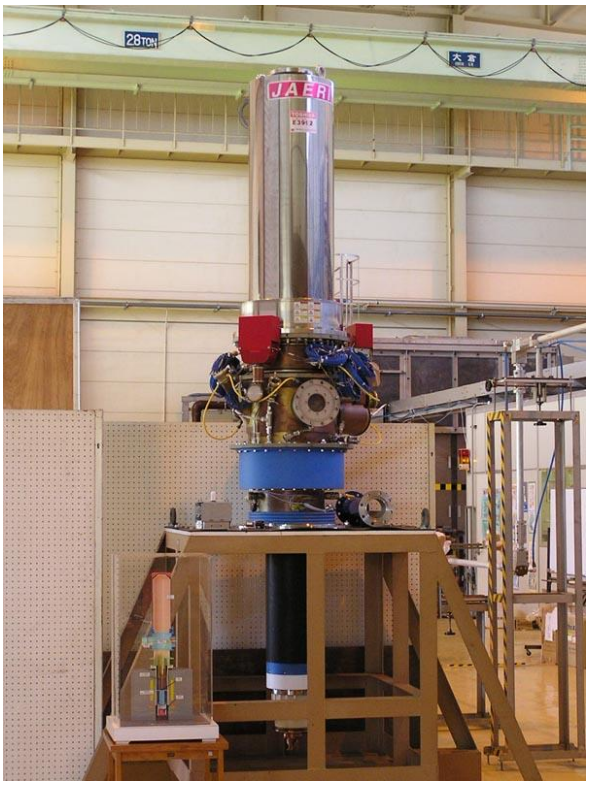

Figure1-3 Gyrotron

A feasibility study of Gyrotron as beam source of BEP was conducted by Jordin T. Kare *et al.*[12] using the NASA Technology Readiness Level (TRL) scale [13]. Because Kare et al. have proposed Microwave thermal rocket (its propulsion principle is different from that of the microwave rocket) they investigated continuous wave (CW) gyrotron. Although we plan to employ pulsed gyrotron, the investigation serves as a useful reference. According to the study, individual 900 kW CW gyrotrons at 110 GHz and 140 GHz are TRL 8: in commercial production, with further development being driven by their application to electron cyclotron-resonance heating (ECH) systems for magnetic confinement fusion experiments. In addition, about apertures and array, Millimeter-wave steerable dish antennas have such an extensive field history that they can reasonably be classed as TRL 9. Therefore, gyrotron is the most promising devise for BEP. However, a launch system array would be unprecedented in size and average power, and in the combination of number of apertures, precision, and tracking requirements. There are still a lot of problems for BEP.

1.3 launch trajectory for Microwave Rocket to space

Katsurayama *et al*. proposed a vertical launch to minimize the development cost of the laser base. The trajectory is shown in Fig. 1-4. On this strategy, the vehicle is boosted by beaming propulsion to reach the orbit beyond the GEO. At the apogee point, the vehicle is kicked to a GTO by an on-board motor and decelerated at the perigee point as well.

Using the trajectory, if the vehicle is boosted to 10.85km/s, necessary velocity increment by the on-board motor will be only 2km/s, which can be achieved by electric propulsion [14].

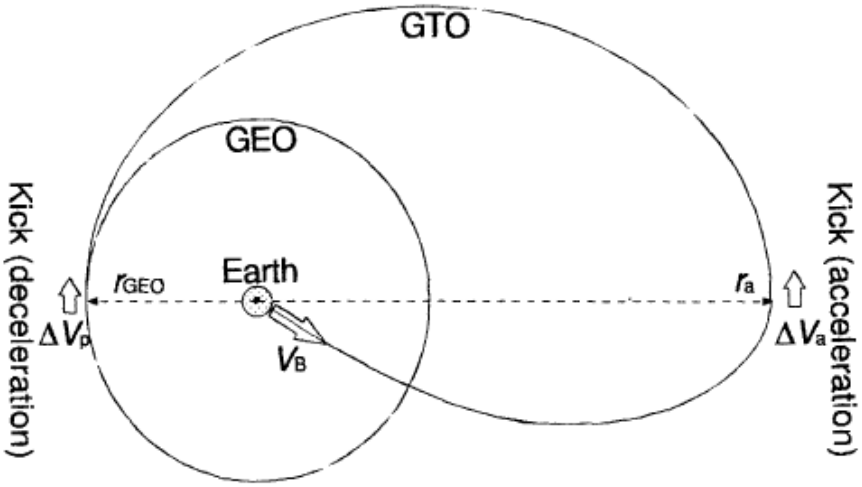

Figure1-4 a trajectory to GEO proposed in ref[14]

1.4 Thrust Generation Model of Microwave Rocket

Figure 1-5 shows the engine cycle of Microwave Rocket, along with the pressure distribution in the thruster, which is similar to a pulse detonation engines [15-16]. The thruster model has open-end and closed-end. The closed-end is called thrust wall and there is beam collector to focus the microwave beam. As the first step of the engine cycle, pulsed microwave beam irradiated form open-end is focused by a collector and generates plasma, driving shockwave (Fig.1-5(1)). Then the plasma and shockwave propagate toward opposite direction of microwave irradiation absorbing the following part of the microwave (Fig.1-5(2)). This phenomenon is called as Microwave Supported Detonation (MSD). The thruster obtains thrust from high pressure behind the shockwave. When the plasma and shockwave reaches thrust-end, an expansion wave starts to propagate to inside of the thruster (Fig.1-5(3-4)). It causes a pressure oscillation in the thruster (Fig.1-5(4-5)). Reed valves are opened by the pressure difference between outside and inside of the thruster and starts to refilling. The engine cycle is repeated.

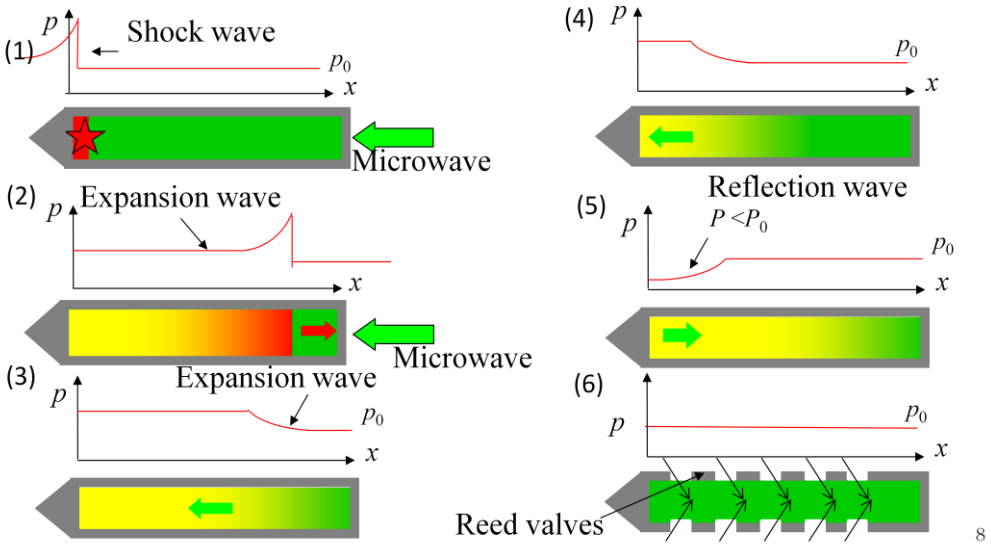

Figure1-5 Engine cycle model focusing thruster.

1.5 Objectives of this study

One of the big challenges of microwave rocket is flight demonstration. In 2009, we conducted the demonstration using 109 g thruster and achieved 1.2 m launch. As a next step, we aim to launch kg order thruster. For the launching, maintaining of thrust is most important element with microwave repetitive radiation. Air-breathing performance by the reed valve affects thrust performance, because after the microwave irradiation, the gas in the inside thruster becomes hot and low and causes thrust depression of next engine cycle.

Therefore the pressure wave dynamics of the inside thruster was investigated using one-dimensional thruster model. The mass flow through the reed valve was analytically estimated and incorporated in the CFD computation and pressure history was calculated.

Then reed valve model was developed to reproduce reed motion responding to pressure difference. Pressure distribution of the inside thruster was computed by two-dimensional thruster model. Mass flow through the reed valve, and reed valve displacement were estimated.

References of chapter 1

[1] Kantrowaitz,A., "Propulsion to Orbit by Ground-Based Lasers", *Astronautics and Aeronautics* **10**(5)74(1972)

[2] L. N. Myrabo : "World record flights of beamed-riding rocket light craft", *American Institute of Aeronautics and Astronautics Paper N*, pp. 2001-3798, 2001

[3] J.P.Knecht and M. M. Micci, "Analysis of Microwave-heated planar propagating hydrogen plasma" AIAA Journal, **26**(2)pp188-194,1988

[4] G. M. Batanov, S. I. Gritsinin, I. A. Kossyy, A. N. Magunov, V. P. Silakov, and N. M. Tarasova. "High pressure microwave discharge". In L.M.Kovrizhnykh, editor, *Plasma Physics and Plasma Electronics*, pp241-282. Nova Science Publishers Commack, 1989.

[5] Y. Oda., K. Komurasaki, K. Takahashi, A. Kasugai, and K. Sakamoto; "Plasma generation using high-power millimeter wave beam and its application for thrust generation", *J. App. Phys.* **100**, 2006, 113307

[6] Y. Shiraishi, Y. Oda, T. Shibata, K. Komurasaki, K. Takahashi, A. Kasugai, and K. Sakamoto, "Air Breathing Processes in a Repetitively Pulsed Microwave Rocket", *AIAA Paper*, 2008, 1085.

[7] Y. Oda, T. Shibata, K. Komurasaki, K. Takahashi, A. Kasugai, and K. Sakamoto, "Thrust Performance of a Microwave Rocket Under Repetitive-Pulse Operation", *J. Propulsion and Power* **25**(1), 2009, pp118-122

[8] K. Sakamoto, A. Kasugai, K. Takahashi, R. Minami, N. Kobayashi and K. Kajiwara : "Achievement of robust high-efficiency 1MW oscillation in the hard-self-excitation region by a 170GHz continuous-wave gyrotron", *Nature Physics*, Vol.3, No.6, pp.411-414, 2007.

[9] HAYASHI Kenichi, KATO Akio, OKUBO Yoshihisa and HIGUCHI Toshiharu," Classic and Novel Electromagnetic Source "The High Power Electron Tube", *J. Plasma Fusion Res* .**86(**10),pp567-575,2010

[10] M. Thumm, "Advanced electron cyclotron heating systems for next-step fusion experiments", *Fusion Engineering and Design*, Vol. 30, 139-170, 1995

[11] A.V. Gaponov-Grekhov, V.L. Granatstein, "Applicationof High-Power Microwaves", *Artech House, Boston, London*,1994.

[12] Jordin T. Kare and Kevin L. G. Parkin, "A Comparison of Laser and Microwave Approaches to CW Beamed Energy Launch" *Beamed Energy Propulsion: Fourth International Symposium*, 2006, American Insititute of Physics 0-7354-0322-8

[13] L. N. Myrabo and J. Benford, "Propulsion of Small Launch Vehicles Using High Power Millimeter Waves",*Intense Microwave Pulses II*, ed. by H. E. Brandt, SPIE Proceedings 2154, Bellingham, WA, 1994, pp. 198-217.

[14] H. Katsurayama, M. Ushio, K. Komurasaki and Y. Arakawa, "**A**nalytical Study on Flight Performance of a RP Laser Launcher", *Beamed Energy Propulsion: Third International Symposium*, 2005, American Insititute of Physics 0-7354-0251-5

[15] T. Endo, J. Kasahara, T. Fujiwara, "Pressure History at the Thrust Wall of Simplified Pulse Detonation Engine", *AIAA J.*, Vol. 42, No. 9, 2004, pp. 1921-1930.

[16] T. Endo, T. Fujiwara, "A Simplified Analysis on a Pulse Detonation Engine Model", *Trans. Japan Soc. Space Sci.* **44**(146), 2002, 217-222

Chapter 2

Proposal of Air-breathing Mechanism using Reed Valves

2.1 Concepts of Air-breathing Mechanism of Microwave Rocket

Techniques of fresh charge into the thruster have been the subject for not only microwave rocket but also Pulse Detonation Engine (PDE) or Pulse Jet Engine (PJE). Various devices, disc valves, rotary valves and reed valves have been investigated [1-3]. Reed valves are used as pressure-driven flow controller and do not require any actuators. Additionally, reed valve systems have the advantage of simple and lightweight.

Figure2-1 shows a reed valve and a thruster model. Reed valves are added on the wall as shown in the figure. After the exhausting the shock wave, pressure oscillation is occur in the thruster (see section1.4). Reed valves open inward the thruster by pressure difference between outside and inside and also close during MSD propagation.

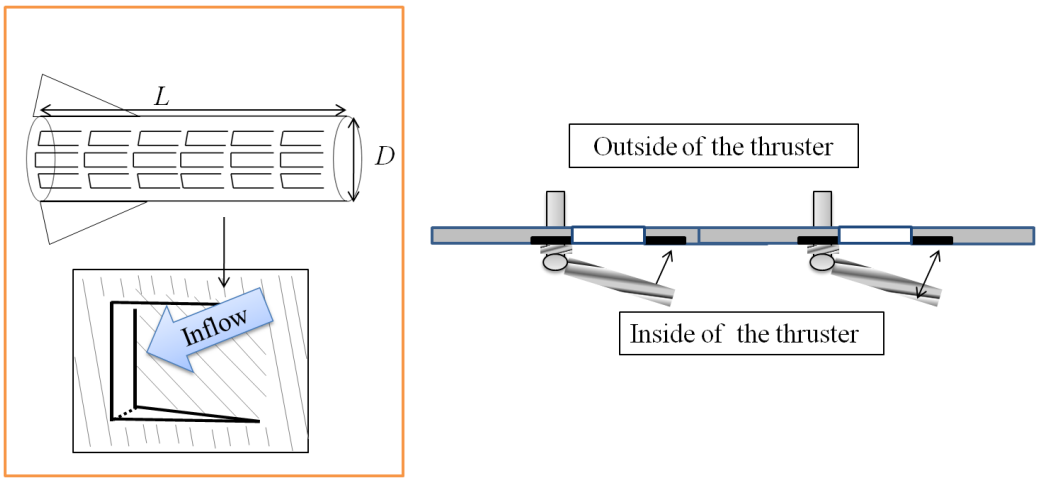

Figure2-1 A reed valve model.

The air-breathing performance is evaluated by the partial filling rate, PFR, which is defined as follows.

$$\mathrm{PFR} = \frac{\text{Refreshed air volume}}{\text{Cylinder volume}} \qquad (2\text{-}1)$$

Shiraishi's experiment [in chapter 1 ref.6] showed that impulsive thrust increases with PFR and that it saturates at FRP=1 as shown in Fig.2-2.

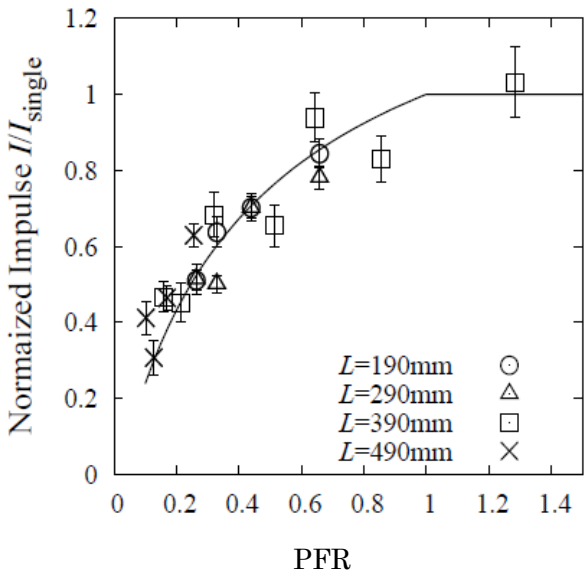

Figure 2-2 Thrust impulse dependence on PFR. Symbols show measurements and a solid line does theoretical prediction [in chapter 1 ref.6].

2.2 Experimental Thruster Model with Reed Valve System

Our research group conducted experiments in 2011 with experimental thruster added reed valves. The inside pressure and thrust impulse is measured. Figure 2-3 shows design of the experimental thruster. The side wall is transparentized to show the inside in the figure. The thruster is constructed by collector, two side-walls added 34 reed valves respectively (the total number of reed valves is 68), two side-walls without reed valves and aluminum frames. The design of microwave collector is illustrated in Fig.2-4. A pressure sensor (Keyence EX-422V) is fixed into the pressure sensor port on collector and measures pressure history at the thrust wall. The thruster was a primary one and was not optimized. Figure 2-5 shows experimental setup.

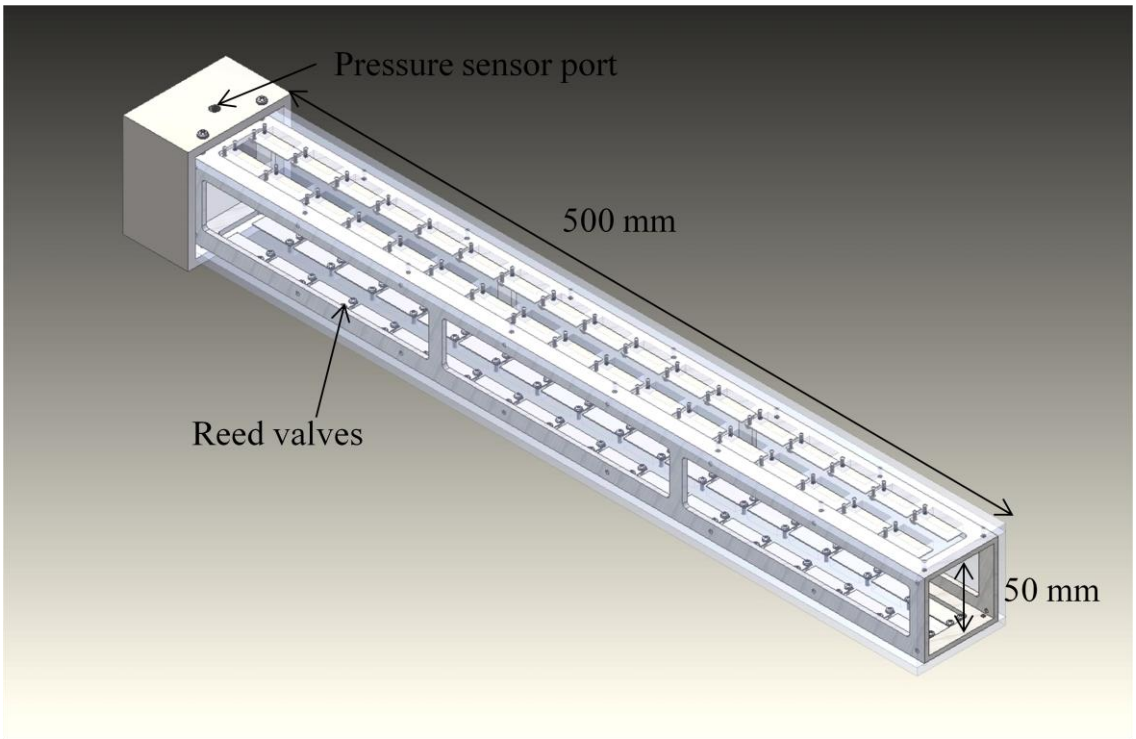

Figure 2-3 Experimental thruster design

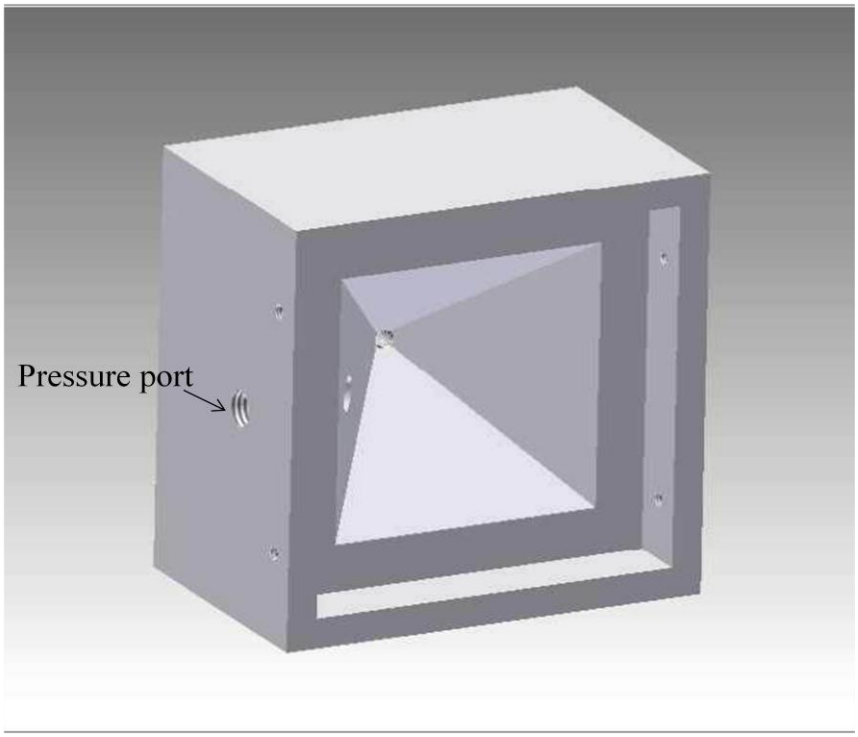

Figure 2-4 Microwave collector design

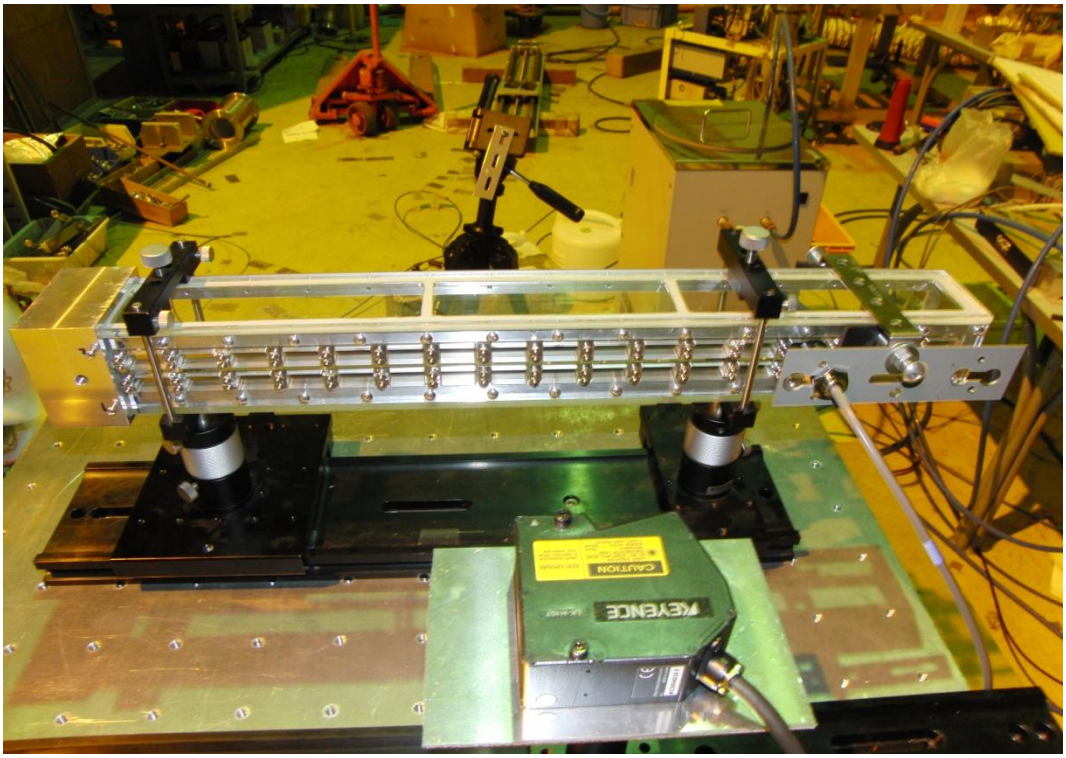

Figure 2-5 Microwave collector design

2.3 Future Model of Microwave Rocket with Air-breathing mechanism

Figure2-6 shows a future model of microwave rocket [4-6]. The model has air intake connecting to reed valves. So the air-breathing microwave rocket uses ram compression flying at high speed. Thus the rocket can breathe ambient air in high altitude depending on the flight speed. When the air-breathing system enables to ingest air in high altitude flight, on-board propellant is used as plasma source. Payloads are enclosed in the body part. And body part also receives microwave as antenna.

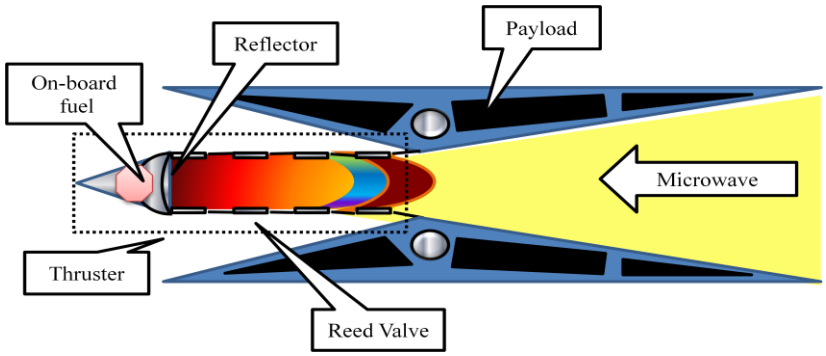

Figure2-6 future model of microwave rocket

References of chapter 2

[1] K. Matsuoka, J. Yageta, T. Nakamichi, J. Kasahara, T. Yajima, T. Kojima, Study on an Inflow-Drive Valve System for Pulse Detonation Engines, *45th AIAA/ASME/SAE/ASEE Joint Propulsion Conference and Exhibit*, *AIAA 2009-5313*,

[2] Fred Schauer, Jeff Stutrud, Royce Bradley,"DETONATION INITIATION STUDIES AND PERFORMANCE RESULTS FOR PULSED DETONATION ENGINE APPLICATIONS" *AIAA 2001-1129*

[3] Paul J. Litke, Frederick R. Schauer, Daniel E. Paxson, Royce P. Bradley,John L. Hoke, "Assessment of the Performance of a Pulsejet and Comparison with a Pulsed-Detonation Engine", 4*3rd AIAA Aerospace Sciences Meeting and Exhibit*,January 10-13, 2005

[4] Masafumi FUKUNARI, Toshikazu YAMAGUCHI, Reiji KOMATSU, Hiroshi KATSURAYAMA, Kimiya KOMURASAKI,Yoshihiro ARAKAWA, "Preliminary Study on Microwave Rocket Engine Cycle" *Plasma Application and Hybrid Functionally Materials*, Vol.20, March 2011

[5] Masafumi FUKUNARI, Reiji KOMATSU, Toshikazu YAMAGUCHI, Kimiya KOMURASAKI, Yoshihiro ARAKAWA, Hiroshi KATSURAYAMA , "Engine Cycle Analysis of Air Breathing Microwave Rocket with Reed Valves", *7th International Symposium on Beamed Energy Propulsion*, Apr.2011

[6] Masafumi FUKUNARI, Hiroshi KATSURAYAMA, Toshikazu YAMAGUTCHI, Kimiya KOMURASAKI, Yoshihiro ARAKAWA, "Analytical Study on Flight Performance of Microwave Rocket"、*the 28th International Symposium on Soace Technology and Science*, June, 2011

Chapter 3

Calculation: One-dimensional Thruster Model

In the chapter, using one-dimensional CFD calculation, pressure oscillation inside the thruster was reproduced. Effects of refilling were incorporated by setting reed valve open ratio α. The mass flow through the reed valve is computed and assessed by PFR (see eq.2-1). Tendencies In addition impulsive thrust is estimated.

3.1 Computational Domain and Initial Condition

Computational domain is shown in Fig.3-1. Inside of the thruster model (see section 1.4) is computed. D and L respectively denote the diameter and the length of the cylindrical thruster body.

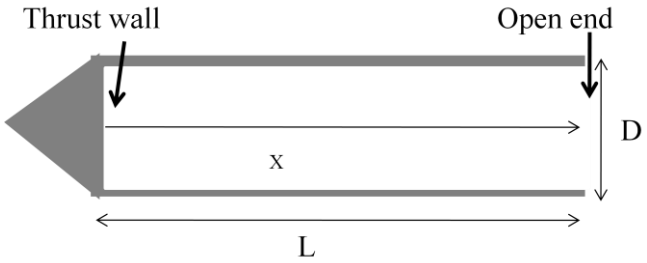

Figure 3-1 one-dimensional thruster model

The pressure distribution in the thruster at when the MSD wave reached the exit end is used as the initial condition for the CFD. Given Chapman–Jouguet [1] detonation at microwave power density, W_d W/m^2, the MSD propagation Mach number M_{msd} is expressed as shown below.

$$M_{msd} = \sqrt{\frac{\left(\gamma^2 - 1\right)}{2a_0^2}\frac{\eta W_d}{\rho_0 M_{msd} a_0} + 1} + \sqrt{\frac{\left(\gamma^2 - 1\right)}{2a_0^2}\frac{\eta W_d}{\rho_0 M_{msd} a_0}} \tag{3-1}$$

Therein, a and η respectively signify the sonic velocity and absorption coefficient. η was set to 0.24 in this computation. Newton–Raphson method was used to solve Eq. (3-2). Here, P, T, and ρ respectively denote pressure, temperature, and density. Respective conditions behind MSD and the expansion wave are shown using subscripts 1 and 2; subscript c denotes the laboratory coordinate system. First, conditions behind MSD are determined as presented in the following equations.

$$P_1 = \frac{\left(1 + \gamma M_{\mathrm{msd}}^2\right)}{\gamma + 1} P_0 \tag{3-2}$$

$$\rho_1 = \frac{(1+\gamma)M_{msd}^2}{\gamma M_{msd}^2 + 1}\rho_0 \tag{3-3}$$

$$M_{C1} = \frac{M_{msd}^2 - 1}{\gamma M_{msd}^2 + 1} \tag{3-4}$$

Second, an expansion wave follows the MSD wave. Conditions behind the expansion wave are presented as follows.

$$P_2 = \left[1 - \frac{\lambda - 1}{2} M_{c1}\right]^{\frac{2\gamma}{\gamma - 1}} P_1 \tag{3-5}$$

$$\rho_2 = \left[1 - \frac{\gamma - 1}{2} M_{c1}\right]^{\frac{2}{\gamma - 1}} \rho_1 \tag{3-6}$$

Time averaged thrust F_{th} is expressed as follows.

$$F_{th} = C_m \Phi_{duty} W_m \tag{3-7}$$

Here, C_m, a momentum coupling coefficient, is defined.

$$C_m = \frac{\text{Cumulative impulse}}{\text{Microwave beamed energy}} \tag{3-8}$$

The engine duty cycle Φ_{duty} is a product of the microwave pulse duration and the pulse repetition frequency. W_m is the microwave power. The optimum microwave pulse width t_{pulse} is determined as shown below.

$$t_{pulse} = \frac{L}{a_0 M_{msd}} \tag{3-9}$$

Here, the engine duty cycle Φ_{duty} is explained as follows.

$$\Phi_{duty} = \frac{t_{pulse}}{t_c} \tag{3-10}$$

In that equation, t_c signifies the engine cycle time.

3.2 Reed Valve model

Air flow through reed valves was estimated analytically. A reed valve model is portrayed in Fig. 3-2. The aperture ratio of the reed valve, α, is defined as presented in Eq. (3-11) below.

$$\alpha = \frac{nA_{\text{reed}}}{A_{\text{wall}}} = \frac{ny(l+w)}{\pi DL} \tag{3-11}$$

In that equation, A_{reed} and A_{wall} respectively signify the opening area of the reed valve and a side area of the thruster. Furthermore, l, w, y, and n respectively stand for the length, width, and tip displacement of a reed and the number of reeds.

The air flow per unit area through a reed valve is a function of the pressure ratio P_{in}/P_0 and temperature as presented in the equations below [2].

$$\dot{m}_{\text{u}} = \beta\rho_0 P_0 \sqrt{\frac{T_0}{T_{\text{in}}}} \qquad (P_{\text{in}}/P_0 < b)$$

$$\dot{m}_{\text{u}} = \beta\rho_0 P_0 \sqrt{\frac{T_0}{T_{\text{in}}}} \sqrt{1-\left(\frac{P_{\text{in}}/P_0 - b}{1-b}\right)^2} \qquad (1>P_{\text{in}}/P_0>b) \tag{3-12}$$

Subscripts 0, in, and reed respectively represent the conditions outside and inside of the thruster, and the inflow through a reed valve.

Conditions outside the thruster are assumed as atmospheric air conditions, P_0=1 atm and T_0=298.15 K. The reed valve mechanical vibration is neglected and a reed valve is open only while P_{in}/P_0<1. In the equations, β and b respectively express the effective cross section factor and critical pressure ratio, as measured in Komatsu's experiments [3]. Figure 3-3 shows calculated results of the air flow per unit area through a reed valve.

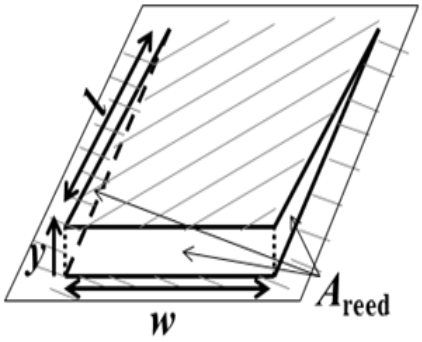

Figure 3-2 Reed Valve

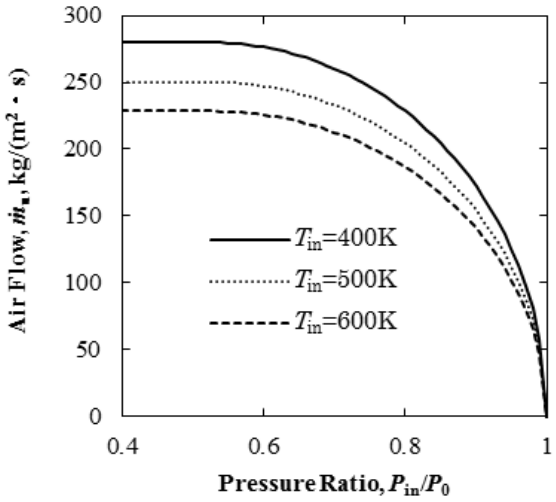

Figure 3-3 Incoming air flow per unit area through a reed valve

The pressure and the density on the reed aperture P_{reed} and ρ_{reed} are determined as presented below.

$$\begin{cases} \rho_{\text{reed}} = \rho_0 \, b^{\frac{1}{\gamma}} \\ P_{\text{reed}} = bP_0 \end{cases} \qquad (P_{in}/P_0 < b)$$

$$\begin{cases} \rho_{\text{reed}} = \rho_0 \left(\dfrac{P_{in}}{P_0} \right)^{\frac{1}{\gamma}} \\ P_{\text{reed}} = P_{\text{in}} \end{cases} \qquad (1 > P_{in}/P_0 > b) \qquad (3\text{-}13)$$

The partial filling rate is computed as follows.

$$\text{PFR} = \frac{\alpha \pi D \int_0^t \int_0^L \frac{\dot{m}_u}{\rho_{\text{reed}}} dx dt}{(D/2)^2 \pi L} = \frac{\frac{4\alpha}{D} \int_0^t \int_0^L \frac{\dot{m}_u}{\rho_{\text{reed}}} dx dt}{L} \qquad (3\text{-}14)$$

3.3 Computational Method

One-dimensional Euler equations inside the thruster tube were solved. With the axial coordinates *x*, the governing equations are given as follows.

$$\frac{\partial Q}{\partial t} + \frac{\partial E}{\partial x} = 4 \frac{\alpha}{D} S \qquad (3\text{-}15)$$

Some variables used for the equation are the following.

$$Q = \begin{bmatrix} \rho \\ \rho u \\ e \end{bmatrix}, \quad E = \begin{bmatrix} \rho u \\ \rho u^2 \\ (e+p)u \end{bmatrix} \tag{3-16}$$

Total energy e is calculated as shown below.

$$e = \frac{p}{(\gamma - 1)} + \frac{\rho u^2}{2} \tag{3-17}$$

The state equation is expressed as the following.

$$P = \rho RT \tag{3-18}$$

Therein, the specific heat ratio of air γ is 1.4; the gas constant R is 287 J/(kg K).

Using the air flow properties calculated in the prior section, the source term is expressed as follows.

$$S = \begin{bmatrix} \dot{m}_u \\ 0 \\ \dfrac{\gamma}{\gamma - 1} \dfrac{P_{reed}}{\rho_{reed}} \dot{m}_u + \dfrac{1}{2} \dfrac{\dot{m}_u^3}{\rho_{reed}^2} \end{bmatrix} \tag{3-19}$$

A numerical flux was computed using an AUSM-DV scheme. Time integration was conducted using a two-stage Runge–Kutta method [4-6].

3.4 Calculation Result and Discussion

At first, computed pressure histories at the thruster wall without reed valves was compared with experimental result in Figure 3-4. The results show good agreement.

Figure 3-5 shows the computed pressure histories with reed valves. The pressure oscillation is damped with large α. Figure 3-6 shows PFR history, PFR starts to increase at around 1.7 ms, at which time an expansion wave reached the thrust wall and reflected, creating considerable negative pressure behind it. PFR asymptotically approaches a certain line at α = 0.08, because at the point, pressure oscillation occurs a little, apparently in Fig 3-5.

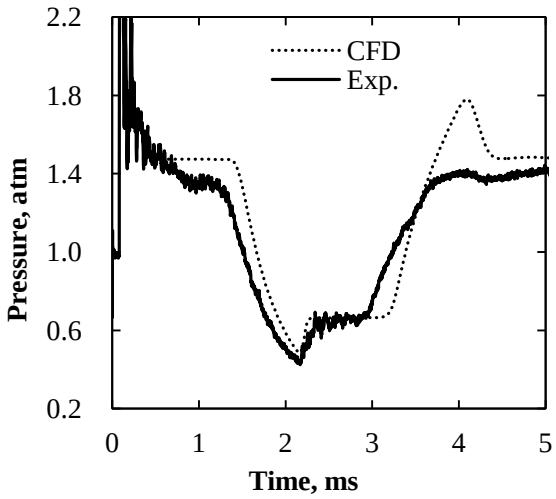

Figure 3-4 Measured and computed pressure histories at the thruster wall without reed valves. L=397.5 mm, D=60 mm and W_m =800 kW

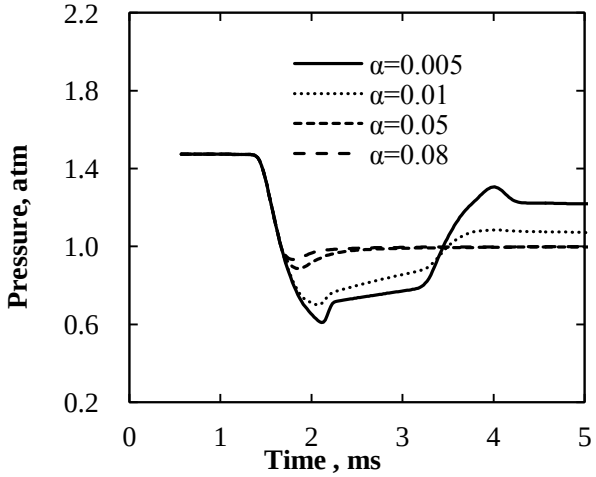

Figure 3-5 Computed pressure histories on the thruster wall with reed valves.

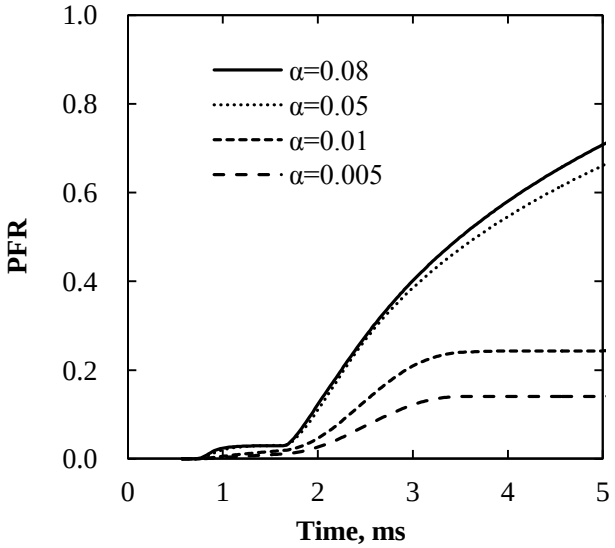

Figure 3-6 Computed pressure histories on the thruster wall with reed valves.

Figure 3-7 shows the comparison of calculation and experiment. using these results α was estimated as $\alpha \approx$ 0.006.

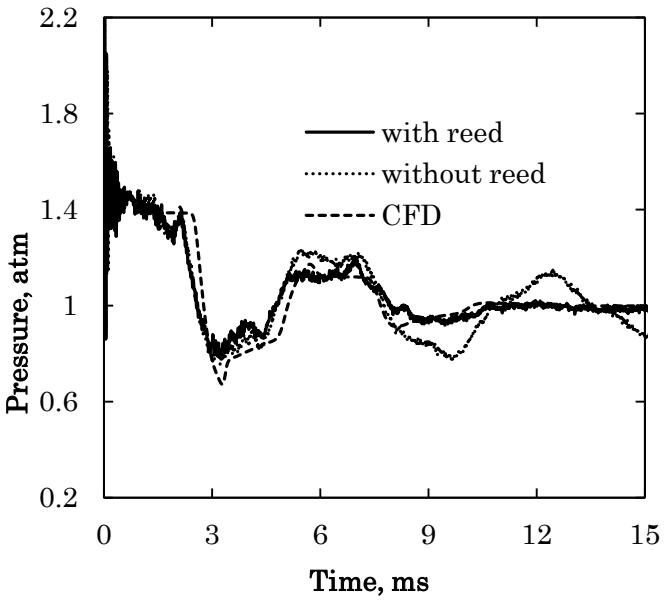

Figure 3-7 Computed pressure histories on the thruster wall with reed valves.

Using Shiraishi's experiment result (see section 2-1) impulsive thrust is estimated at 20 N in multiples operation.

3.5 Summary and Conclusion

The one-dimensional analytical model of the thruster was developed. The comparison of pressure history at the thrust wall between calculations and experiments shows good agreement. Then tendency of the pressure history with reed valves was computed. As a result it is observed that pressure oscillation is damped with large α because of refilling. PFR starts to increase at around 1.7 ms, at which time an expansion wave reached the thrust wall and reflected, creating considerable negative pressure behind it. This period depend on velocity of the expansion wave and also thruster length. For sufficient refilling each refilling period should be greater than the period which the expansion wave reaches to thrust wall. Because typical microwave repetitively frequency is 50~200 Hz, the period can be neglected in this case. However in the case of using long thruster, the period gives advice.

The calculation result was compared with experimental results, and it is appeared that α of the experimental thruster was estimated around 0.006. At first α had been expected as around 0.04 (assuming 2 mm reed tip lift). The value of α of the experimental result was too small. So we have to investigate the matter.

Using Shiraishi's experiment result (see section 2-1) impulsive thrust is estimated at 20 N in multiples operation.

References of chapter 3

[1] 疋田　強、秋田　一雄、改訂　燃焼概論、標準応用化学講座 19、コロナ社、pp102-pp118

[2] K. Kawashima, Y. Ishii, T.Funaki, T.Kagawa, "Determination of flow characteristics of pneumatic valves by charge method using isothermal chamber", *The Japan Fluid Power System Society*, (in Japanese), Vol. **34**, No.2, 2003, pp8-13

[3] R. Komatsu, "Air-breathing System on Microwave Rocket with Reed Valves and Its Future Possibility", *ISTS Paper*, 2011, b-41s

[4] Y. Wada, and M. S. Liou, "A Flux Splitting Scheme with High-Resolution and Robustness for Discontinuities", *AIAA Paper*, 1994, 94-0083

[5] Akiko Matsuo, Toshi Fujiwara, "Numerical Investigation of Standing Oblique Detonation Supported by Two-Dimensional Blunted Wedge", *Trans. Japan Soc. Aero. Space Sci.* **36**(111)

[6] 北村圭一, 嶋英志," AUSM 族スキームの新しい圧力流束：極超音速空力加熱計算のための衝撃波安定, 全速度数値流束の開発に向けて", *第 24 回数値流体力学シンポジウム*,B12-3

[7] 高崎浩一, 大竹邦彦, 小川哲, "圧縮性 NS コード FIVAD の 機体伝熱問題に対する応用について", 航空宇宙技術研究所資料, TM-729

Chapter 4

Calculation: Reed Valve Model and Two-dimensional Thruster Model

One-dimensional model can represent tendency of pressure history and mass flow with low calculation cost. In this chapter, a reed valve model was calculated to investigate mass flow through the reed valve considering reed motion and pressure distribution..

4.1 Calculation Domain and Initial Condition

Figure 4-1 shows calculation domain. The domain is plane symmetry and included free area around open-end. The design of the thruster is set as same as the experimental thruster (see section 2.2). The initial condition of inside the thruster is same as section 3.1. The initial condition of free area is standard atmospheric air, pressure P = 1 atm, temperature T = 300 K. Reed valve is added on the side wall of the thruster.

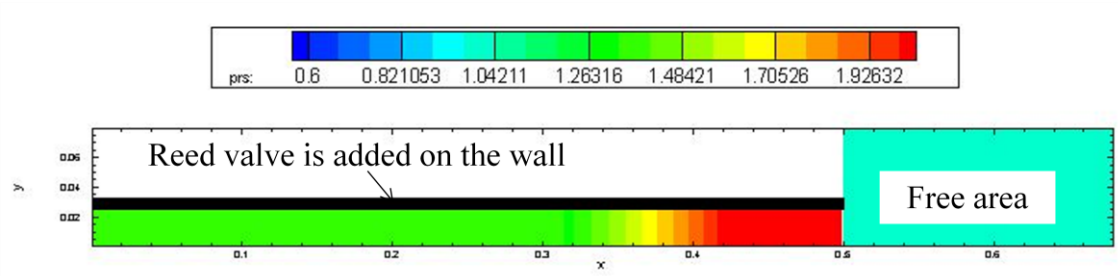

Figure 4-1 Calculation domain of the thruster and free area. The domain is plane symmetry.

4.2 Reed Valve Model

Reed valve are found in many fields of techniques, compressors [1-4], jet engine and two-stroke engine [5-15]. In the field of two-stroke engine, reed valves are fitted in engines of the crankcase compression two-stroke cycle engine. Blair *et al*. proposed a two-dimensional model based on beam theory in 1978-79 [5-6]. And the model improved by Fleck et al. taking into the effect of tapered, and width and non-uniform load [7-8]. For compressor, one of the most complete simulations of gas pressure oscillation is proposed by Brablik [1].

From considerations of the theory of transverse vibrations of vibrations of a loaded beam, the response of a cantilever reed valve in unsteady gas dynamic regions can be described by the equation

$$\rho_{rd} A_{rs} \frac{\partial^2 y(x,t)}{\partial t^2} + E_{rd} I \frac{\partial^4 y(x,t)}{\partial x^4} = 0 \qquad (4\text{-}1)$$

where ρ_{rd}, A_{rs}, E_{rd}, I, y, x and t are material density of the reed petal, reed cross-section, Young's module, second moment of area, reed tip displacement, the axial coordinates on the reed valve and time, respectively. The equation of free vibration will have a solution of the type

$$y = Y(x)e^{i\omega t} \tag{4-2}$$

Where the function $Y(x)$ is the form and ω is angular frequency.

$$Y(x) = A\cos\lambda x + B\sin\lambda x + C\cosh\lambda x + D\sinh\lambda x \tag{4-3}$$

where

$$\lambda = \sqrt[4]{\frac{\rho_{rd} A_{rs}\omega^2}{E_{rd} I}} \tag{4-4}$$

and A, B, C and D are constant. Inserting the end conditions for a cantilever,

$$y = \frac{dy}{dx} = 0 \quad (x = 0), \quad \frac{d^2y}{dx^2} = \frac{d^3y}{dx^3} = 0 \quad (x = l) \tag{4-5}$$

Here, l is a reed petal length. The frequency equation is

$$1 + \cos\lambda l + \cosh\lambda l = 0 \tag{4-6}$$

solving for the first 3 roots. Solutions of frequency equation for Clamped-Free Beam are

$$\lambda_1 l = 1.875, \quad \lambda_2 l = 4.694, \quad \lambda_3 l = 7.555 \tag{4-7}$$

ω is determined by

$$\omega_i = (\lambda_i l)^2 \sqrt{\frac{E_{\mathrm{rd}} I}{\rho_{\mathrm{rd}} A_{\mathrm{rs}} l^4}} \tag{4-8}$$

The frequency of the vibration f_i is given by

$$f_i = \frac{\omega_i}{2\pi} = \frac{(\lambda_i l)^2}{2\pi} \sqrt{\frac{E_{\mathrm{rd}} I}{\rho_{\mathrm{rd}} A_{\mathrm{rs}} l^4}} \tag{4-9}$$

After simplification the mode shape reduces to

$$Y_i(x) = \cosh\lambda_i x - \cos\lambda_i x - \sigma_i(\sinh\lambda_i x - \sin\lambda_i x) \tag{4-10}$$

where

$$\sigma_i = \frac{\sinh\lambda_i l - \sin\lambda_i l}{\cosh\lambda_i l - \cos\lambda_i l} \tag{4-11}$$

Reed tip displacement is given by

$$y(x,t)=\sum_i Y_i(x)q_i(t) \tag{4-12}$$

[5].

The following model is derived by Paul [1]. The valve of the principle coordinate q_i is found from the equation in consideration of damping, ignoring high order modes.

$$\frac{\partial^2 q(t)}{\partial t^2}+2\omega\xi_{eff}\frac{\partial q(t)}{\partial t}+\omega^2 q(t)=\omega^2 G(y)\Delta P \tag{4-13}$$

ξ_{eff} is damping coefficient determined by

$$\xi_{eff}=C_1+\frac{\dot{y}}{C_2}\quad(\dot{y}(t)\geq 0) \tag{4-14}$$

$$\xi_{eff}=\frac{C_3 y}{C_4}\quad(\dot{y}(t)<0) \tag{4-15}$$

where

$$C_1=0.75、\quad C_2=0.2、\quad C_3=1.25、\quad C_4=0.06 \tag{4-16}$$

Although coefficients are not accurate, the results show reasonable agreement with experiments.

ΔP represents applied load per unit area and function $G(y)$ is flow force area function. Even if the pressure difference between outside and inside of the reed valve is same, force loading on reed depend on reed displacement. The function $G(y)$ is determined by

$$G(y)=\frac{\left[B(y)\int_0^l Y(x)dx\right]}{\omega^2\rho_{rd}A_{rd}l\left[\int_0^l Y(x)^2dx\right]}\Delta P \tag{4-17}$$

Here, B(y) is effective force area and defined as

$$B(y)=bl\cos(\theta)$$
$$\theta=\arctan(y/l) \tag{4-18}$$

where b and l are width and length of the reed valve, respectively. Finally, the reed motion is approximated that the reed has spring and damper at reed tip. The image of the reed valve model is shown in figure 4-2.

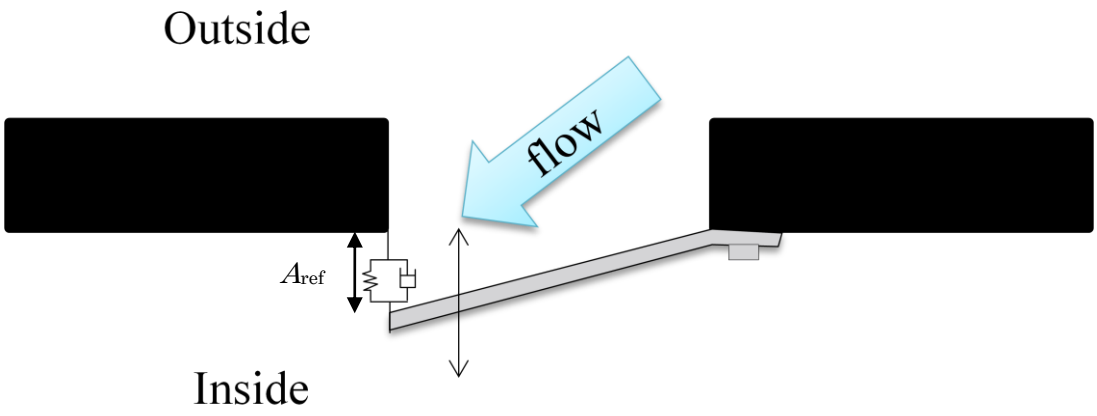

Figure 4-2 Schematic of spring-damper model of the reed valve

Mass flow $\dot{m}$ through the reed vale is expressed by

$$\dot{m} = \frac{C_d A_{ref} P_{out}}{\sqrt{RT_{out}}} \sqrt{\frac{2\gamma}{(\gamma-1)} \left\{ \left(\frac{P_{in}}{P_{out}} \right)^{\frac{2}{\gamma}} - \left(\frac{P_{in}}{P_{out}} \right)^{\frac{\gamma+1}{\gamma}} \right\}} \qquad (4\text{-}19)$$

where C_d and A_{ref} are discharge coefficient and reference area of the reed (see Fig.4-2). The experimental evaluation of C_d was carried out at the fluid dynamics lab of the University of Perugia. The reed device was arranged on the steady state flow test bench. The position of the reed was maintained by means of a low intrusive steel needle hinged as the plate tip, while the lift of the reed tip was checked with a micrometer. The measurements were carried out varying the tip lift, both in intake and exhaust mode with pressure drop of 100 mbar. Numerical simulation was also carried out in steady state condition [9].However the discharge coefficient can vary by reed petal geometry and pressure difference. Therefore, to investigate the discharge coefficient of our reed valve system the reed valve model was integrated in CFD calculation. For the calculation the main character of the reed valve is set as same as experiment which is shown in table 1

Table 1. Main character of the reed valve.

Material	sus304CSP,
Length *l*	20 mm
Width *w*	10 mm
Thickness s	0.2 mm
Material density ρ_{rd}	7800 kg/m^3
Young's Module E_{rd}	2.0E+11 Pa

The computation set up is shown in figure 4-3. The reed is located on top wall. Actually the reed

valve added on the thruster is separated in center but for simplicity the bridge between petals was neglected. In this calculation reed tip displacement is fixed. Figure 4-4 show computational grid.

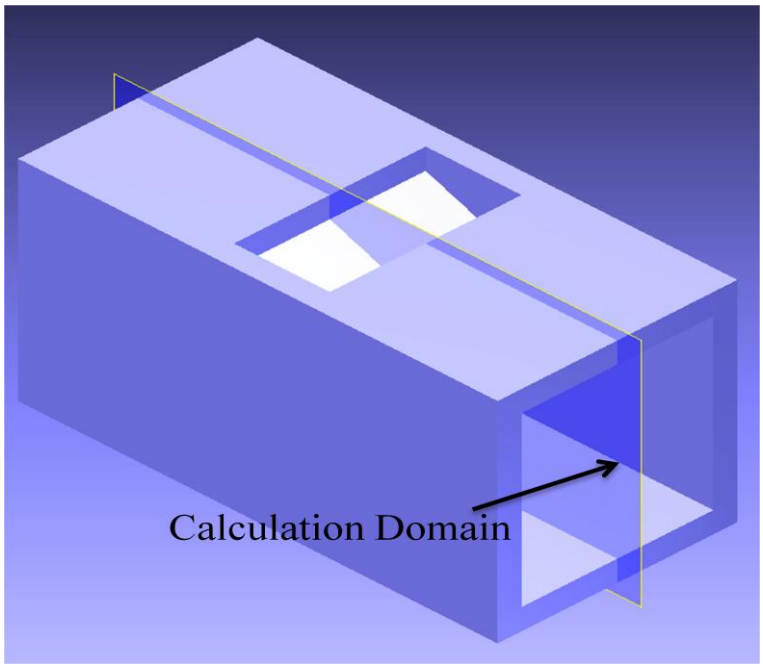

Figure 4-3 Computational set up of Reed valve CFD calculation

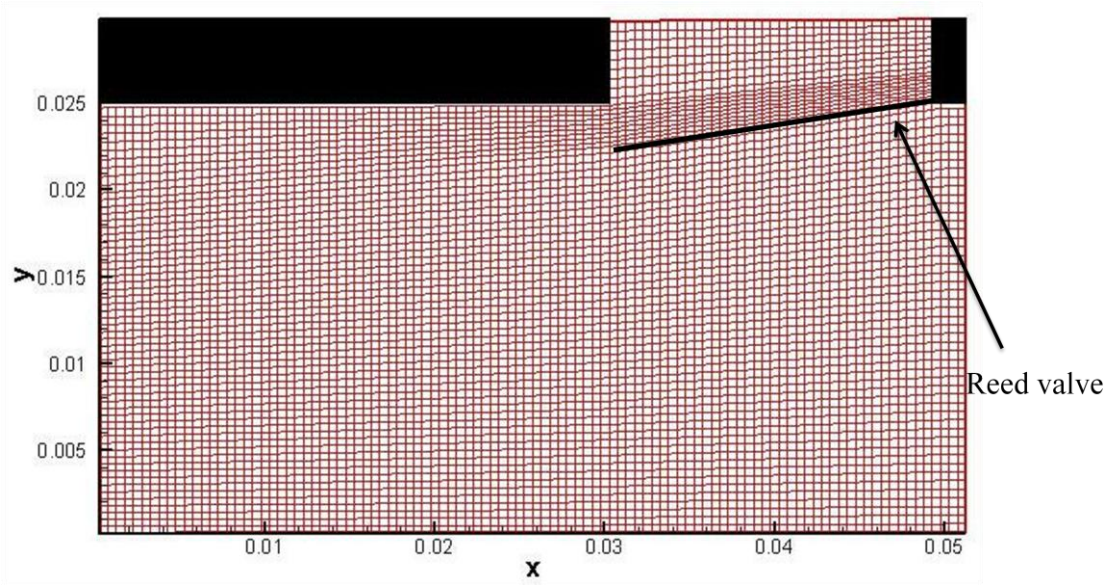

Figure 4-4 Computational grid

Figure 4-5 denotes predicted the discharge coefficient vs. reed tip displacement. Marks and solid line show calculation result and fitted curve determined by

$$C_d = 0.0014y^5 + 0.0213y^4 + 0.1259y^3 + 0.3537y^2 + 0.4605y + 0.4676 \quad (4\text{-}20)$$

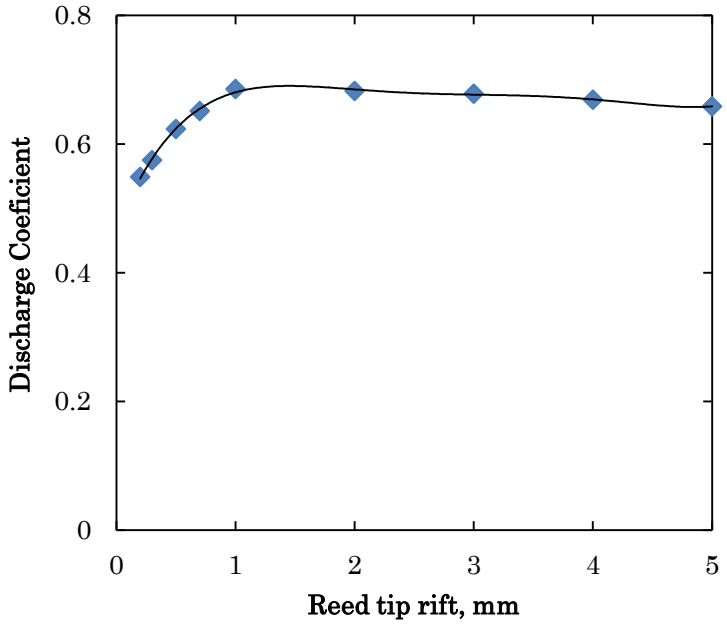

Figure 4-5 Predicted discharge coefficient

The pressure contour of the reed valve is shown in Fig.4-6~Fig. 4-7. Figure 4-6 shows starting point of refilling. There is negative pressure at under the reed petal. Figure 4-17 shows stream line. Apparently the flow once collides to reed petal. However, the flow is squeezed at the boundary between outside and inside.

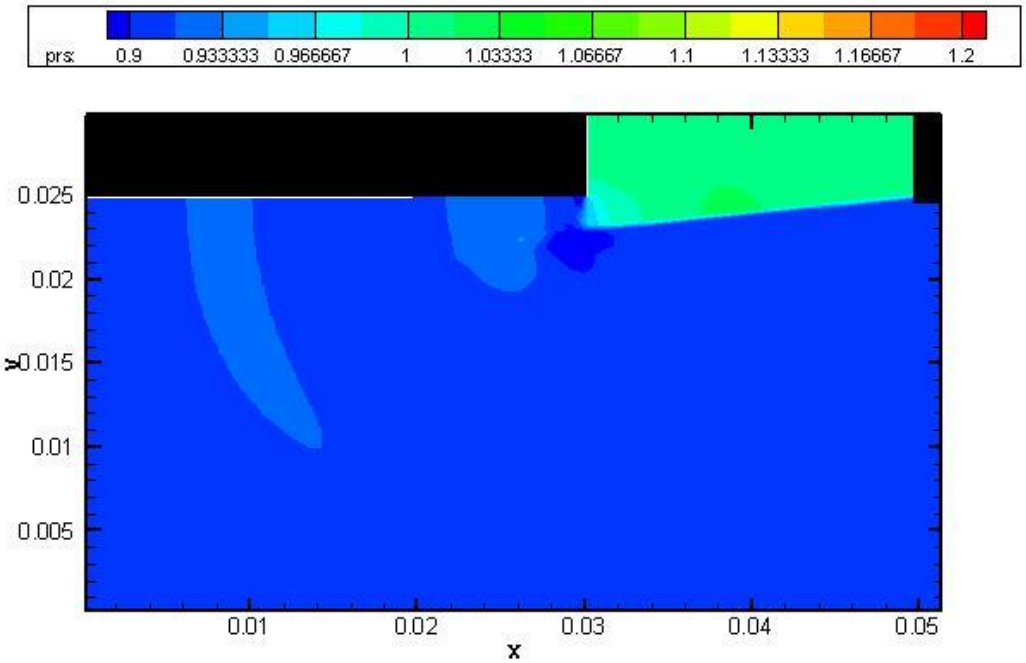

Figure 4-6 Calculated pressure contour at time =0.1 ms.

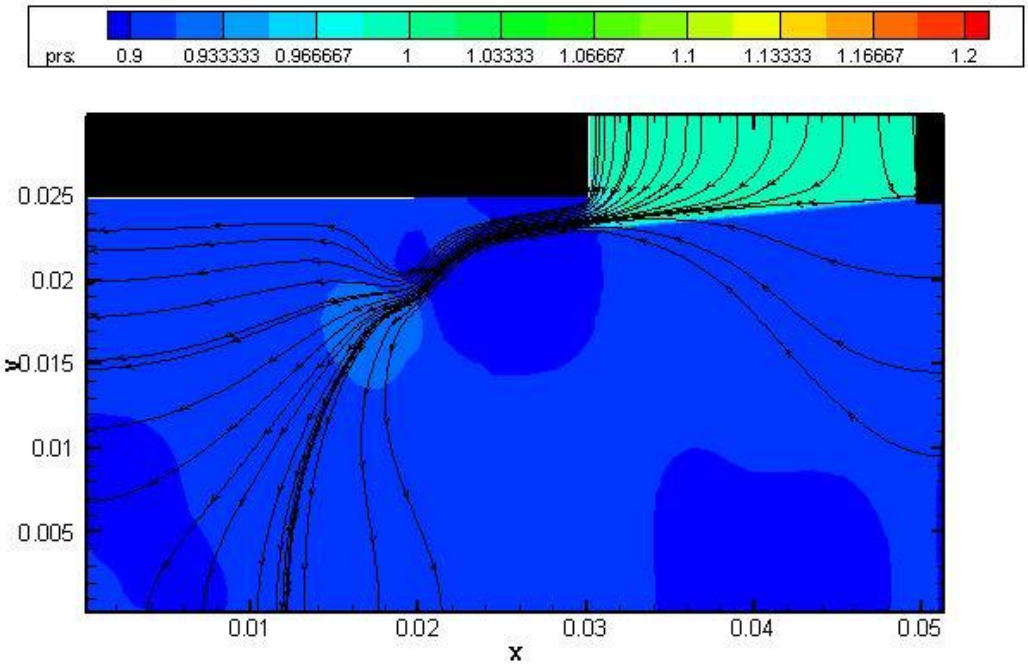

Figure 4-7 Calculated pressure contour at time =0.28 ms. With streamline

4.3 Calculation method of the two-Dimensional Thruster and the Reed Valve.

In order to find some barometers, the reed valve model, Eq. (4.17) is considered. For simplicity, dumping term is neglected. Then organizing the equation to investigate of the reed motion, the equation becomes

$$\frac{\partial^2 q(t)}{\partial t^2} = \frac{\left[B(y)\int_0^l Ydx\right]}{\rho bhl\left[\int_0^l Y^2 dx\right]}\Delta P - \left[(\lambda_i l)^2\sqrt{\frac{EI}{\rho A l^4}}\right]^2 q(t) \tag{4-21}$$

Here,

$$\frac{\int_0^l Ydx}{\int_0^l Y^2 dx} = const \approx 0.7830 \tag{4-22}$$

which numerically was confirmed. Given material of the reed, Young's module and density are decided and Eq.(4-21) is reduced as

$$F = \frac{\cos\theta}{h}\Delta P - \frac{E_c}{\phi}\frac{h^2}{bl^3}q(t) \tag{4-23}$$

where E_c, Φ are constant term and F is

$$F = \frac{1}{\phi}\frac{\partial^2 q(t)}{\partial t^2} \tag{4-24}$$

First considering valve opening, according to Eq.(4-23), it is found that a combination small h and large b and l could be better. However ω increase with increase b and l, which causes that the reed valve does not close in the case of negative pressure. Then, therefore, balance at the design point is considered. The design point has arbitrary property. For instance, given design point as ΔP = 0.1atm (average negative pressure of the inside thruster), b = 10 mm, l = 20 mm, and average reed tip displacement y = 2 mm, the thickness is decided as 0.1 mm. In the calculation reed material was same as table1.

4.4 Calculation method of the two-Dimensional Thruster and the Reed Valve.

Governing equation are given by follows

$$\frac{\partial Q}{\partial t} + \frac{\partial E}{\partial x} + \frac{\partial F}{\partial y} = 0 \qquad Q = \begin{bmatrix}\rho\\ \rho u\\ \rho v\\ e\end{bmatrix} \text{、} E = \begin{bmatrix}\rho u\\ \rho u^2 + p\\ \rho vu\\ (e+p)u\end{bmatrix} \text{、} F = \begin{bmatrix}\rho v\\ \rho uv\\ \rho v^2 + p\\ (e+p)v\end{bmatrix} \tag{4-25}$$

where *v* is vertical velocity. A numerical flux was computed using an AUSM-DV scheme and time integration was conducted using a two-stage Runge–Kutta method as same as chapter 3. For high accuracy MUSCL method was used.

For analysis of fluid in non-orthogonal grid using finite volume method, it is necessary to construct generalized coordinate system of the type

$$\xi = \xi(x, y), \qquad \eta = \eta(x, y) \tag{4-26}$$

Considering coordinate conversion, for instance convection term of x direction E is expressed as

$$\frac{\partial E}{\partial x} = \frac{\partial \xi}{\partial x}\frac{\partial E}{\partial \xi} + \frac{\partial \eta}{\partial x}\frac{\partial E}{\partial \eta} \tag{4-27}$$

Organizing the equation, the conservation form of the Euler equations in generalized coordinates is

$$\frac{\partial \hat{Q}}{\partial t} + \frac{\partial \hat{E}}{\partial \xi} + \frac{\partial \hat{F}}{\partial \eta} = 0 \qquad \hat{Q} = \frac{1}{J}\begin{bmatrix} \rho \\ \rho u \\ \rho v \\ e \end{bmatrix} \quad 、 \hat{E} = \frac{1}{J}\begin{bmatrix} \rho U \\ \rho u U + \xi_x p \\ \rho v U + \xi_y p \\ (e+p)U \end{bmatrix} 、 \hat{F} = \frac{1}{J}\begin{bmatrix} \rho V \\ \rho u V + \eta_x p \\ \rho v V + \eta_y p \\ (e+p)V \end{bmatrix} \tag{4-28}$$

where

$$\begin{matrix} \xi_x = Jy_\xi \\ \xi_y = -Jx_\eta \end{matrix}, \begin{matrix} \eta_x = -Jy_\xi \\ \eta_y = Jx_\xi \end{matrix}, \begin{matrix} U = \xi_x u + \xi_y v \\ V = \eta_x u + \eta_y v \end{matrix}$$
$$J = \frac{1}{x_\xi y_\eta - x_\eta y_\xi} \tag{4-29}$$

The superscript (^) indicates variable in the generalized coordinates. The Jacobian of the transformation J physically corresponds to the inverse of cell volume. In finite volume method, the average values of the cell are used to represent the currently condition. For the generalized coordinates, because each cell volumes are different, total conservation values are used to calculation.

The numerical flux splitting method, AUSMDV can be applied for the Cartesian coordinates, therefore local Cartesian coordinate is used using the method proposed by W. Kyle Anderson *et al.* [16].

For the purpose of determining a generalized splitting for $\hat{E}$, only the derivatives in the ξ and t direction are considered, while the η derivatives are treated as source terms. For determining the splitting of $\hat{E}$, Eq. (4-23) is transformed by local rotation matrix T given by

$$T = \begin{bmatrix} 1 & 0 & 0 & 0 \\ 0 & \cos\theta & \sin\theta & 0 \\ 0 & -\sin\theta & \cos\theta & 0 \\ 0 & 0 & 0 & 1 \end{bmatrix} \tag{4-30}$$

where

$$\cos\theta = \frac{\xi_x}{|grad\xi|}$$
$$\sin\theta = \frac{\xi_y}{|grad\xi|} \tag{4-31}$$

Multiplication of Eq.(4-28), with the matrix T then yields

$$\overline{Q}_t + \overline{E}_\xi = -T\hat{F}_\eta + T_t\hat{Q} + T_\xi\hat{F} \tag{4-32}$$

where

$$\overline{Q} = T\hat{Q} = \frac{1}{J}\begin{bmatrix} \rho \\ \rho\bar{u} \\ \rho\bar{v} \\ e \end{bmatrix} \tag{4-33}$$

$$\overline{E} = T\hat{E} = \frac{|grad\xi|}{J}\begin{bmatrix} \rho\bar{u} \\ \rho\bar{u}\bar{u} + P \\ \rho\bar{u}\bar{v} \\ (e+p)\bar{u} \end{bmatrix} \tag{4-34}$$

The rotated velocity component $\bar{u}$ is the velocity normal to a line of constant ξ representing the scaled contra variant velocity and $\bar{v}$ is normal to $\bar{u}$.

$$\bar{u} = \frac{\xi_x u + \xi_y v}{|grad\xi|} \tag{4-35}$$

$$\bar{v} = \frac{-\xi_y u + \xi_x v}{|grad\xi|} \tag{4-36}$$

The transformed flux $\hat{E}$ is of the same functional from as the Cartesian flux vector and thus can be split according to any splitting developed for Cartesian coordinates, of course AUSMDV. After replacing the Cartesian velocity components u and v by the rotated velocity $\bar{u}$ and $\bar{v}$, AUSMDV is used to split the flux vector $\bar{E}$. Applying the rotation T to Eq. (4-23), simply allows us tp split the flux vector in a one-dimensional fashion, along a coordinate axis perpendicular to the cell interface. After splitting $\bar{E}$, the appropriate splitting for $\hat{E}$ is determined by applying the inverse transformation matrix T-1 to Eq. (4-27) leading to

$$\hat{Q}_t + \left(\hat{E}^+ + \hat{E}^-\right)_\xi + \hat{F}_\eta = 0 \tag{4-37}$$

with

$$\hat{E}^+ = T^{-1}\overline{E}^+ 、\ \hat{E}^- = T^{-1}\overline{E}^- \tag{4-38}$$

Note that the inverse transformation restores the original form of the equation, i.e., no additional source terms arise and the form of $\hat{F}$ are unaffected this allows a splitting of $\hat{F}$ similar to the splitting of $\hat{E}$ shown above.

4.5 Calculation result and discussion

Figure 4-8 shows reed valve numbering. There are 17 reed valves on the wall (actually each point has two reed valves). Fig.4-9 shows a comparison of reed tip displacement between the computation and the experiment.

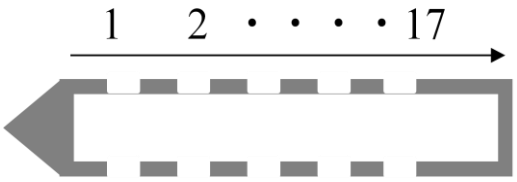

Figure 4-8. Reed valve numberings

In the computation, because reed tip displacement to negative direction did not reproduced, reed opening moment is different. However order of the opening period and the displacement show reasonable agreement.

Reed tip displacements disaggregated by location of the reed valves are illustrated in Fig. 4-10 and Fig. 4-11, which reed shape is set as experimental condition (see table.1). At open end, reed tip open a little and Refilling occurs mainly at around center of the thruster and thrust wall. However in this case the reed tip displacement is small.

Figure 4-12, and figure 4-13 shows reed tip displacement of the reed valve which h = 0.1 mm. Results of h =0.1 mm reaches design point of y = 2 mm.

Table 2 represents comparison a maximum reed tip displacement.

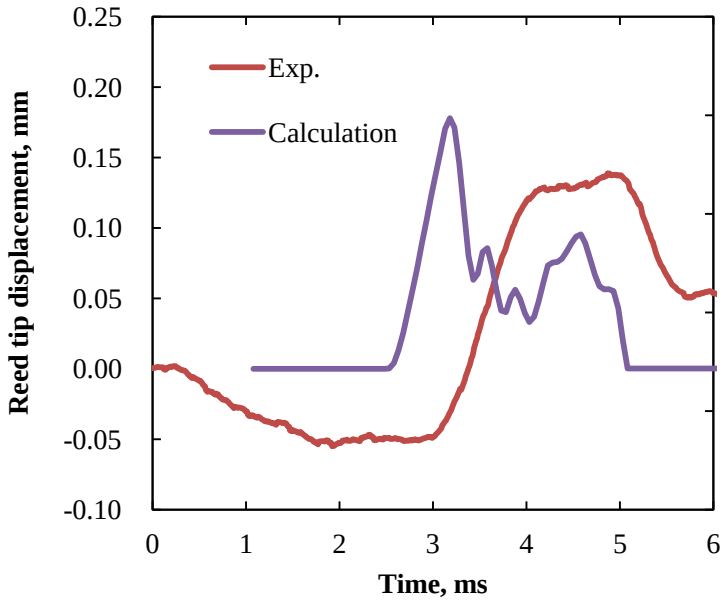

Figure 4-9 Comparison of reed tip displacement between the computation and the experiment

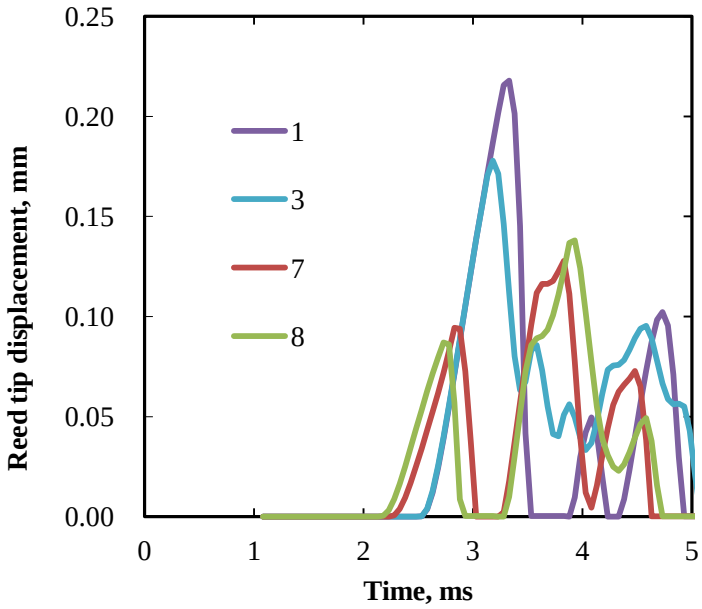

Figure 4-10 Reed tip displacement at around the thrust wall and center of the thruster. *b* = 10 mm, *l* = 20 mm, *h* = 0.5 mm

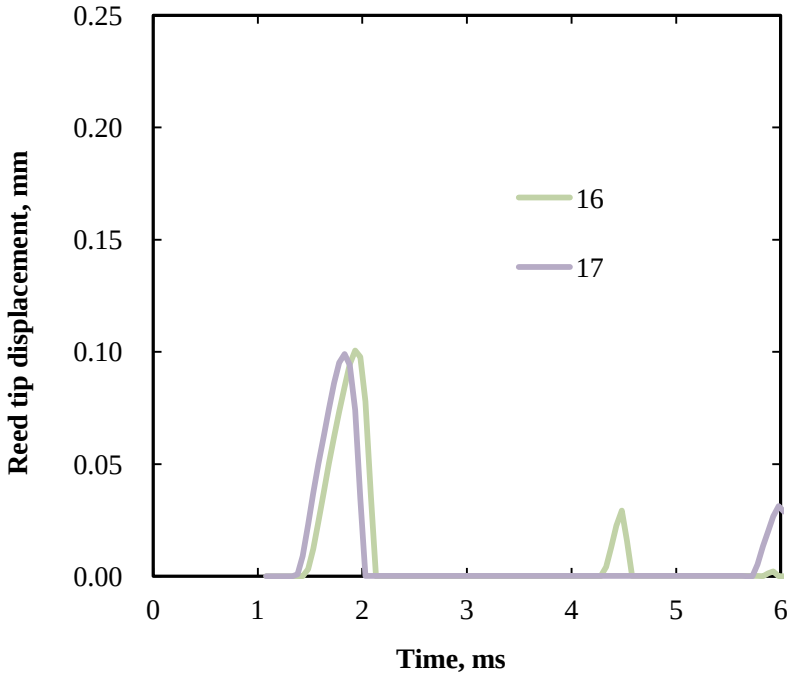

Figure 4-11 Reed tip displacement at around the open end. *b* = 10 mm, *l* = 20 mm, *h* = 0.5 mm

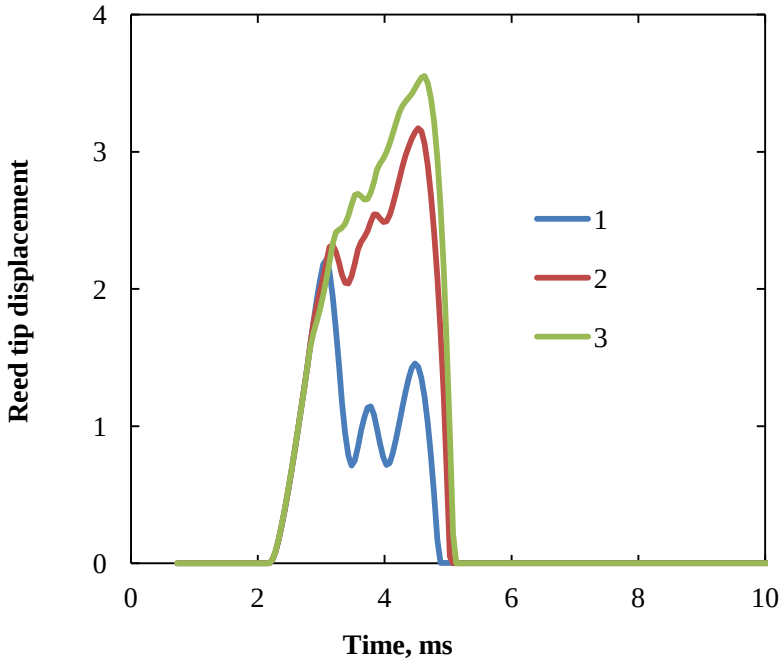

Figure 4-12 Reed tip displacement at around the thrust wall. *b* = 10 mm, *l* = 20 mm, *h* = 0.1 mm

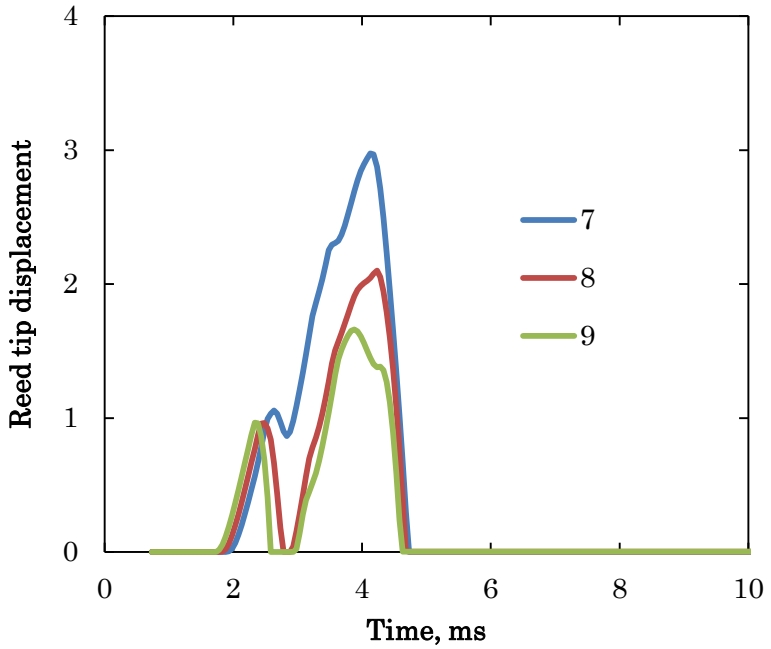

Figure 4-13 Reed tip displacement at around and center of the thruster. b = 10 mm, l = 20 mm, h = 0.1 mm

Table 2. Main character of the reed valve.

Thickness	**Maximum displacement**
0.5mm（experiment）	0.23 mm
0.1 mm	3.5mm

Mass flow through the reed valve of h = 0.5 mm and h = 0.1mm are shown in Fig.4-14 and Fig.4-15 as PFR. Using h = 0.1 mm reed valve, PFR becomes 100 times lager. And as expected from calculated reed tip displacement, PFR at open end is a little. However refilling from open end occur at open end.

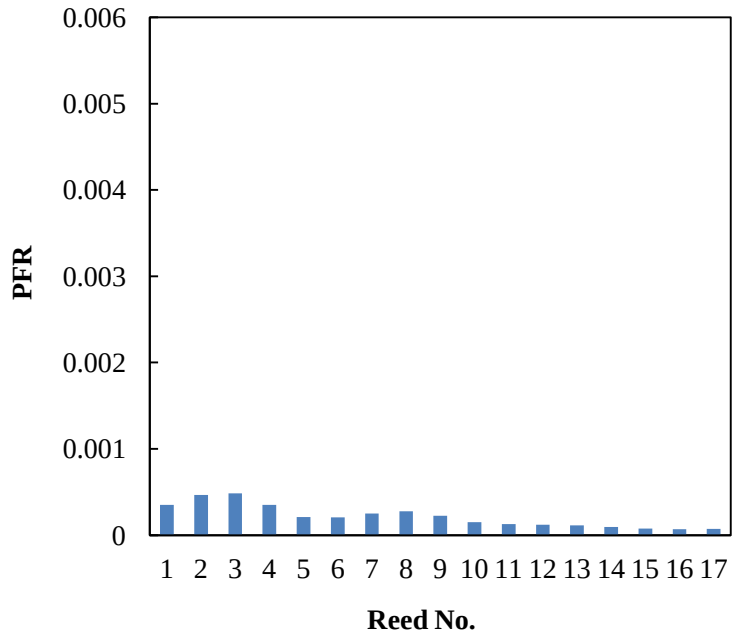

Figure 4-14 PFR of each reed valves, Time = 5ms, *h*=0.5 mm

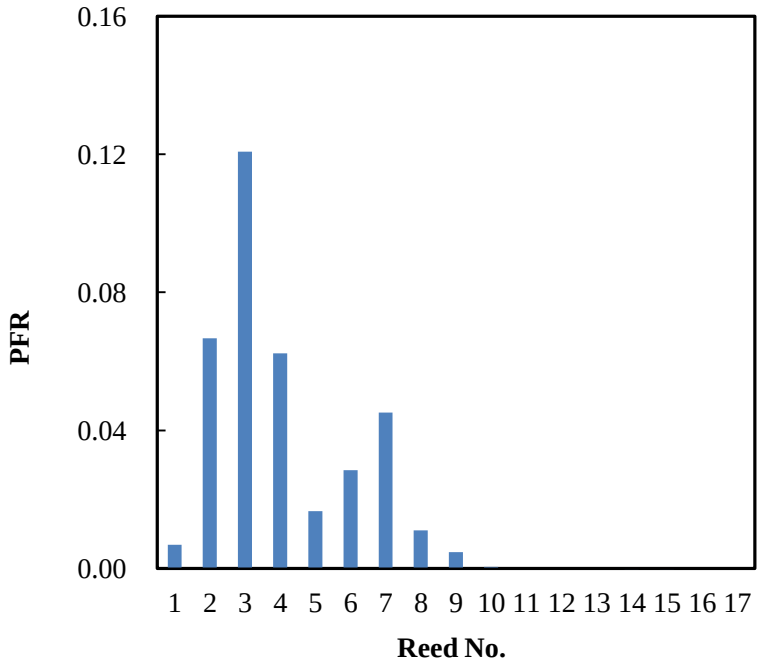

Figure 4-15 PFR of each reed valves, Time = 5ms, *h*=0.1 mm

The pressure contour of the thruster is shown in Fig.4-16~Fig. 4-18. In Figure 4-16, shock wave is exhausted and diffused into free area. In Figure 4-17, the expansion wave is propagating in the thruster accompanying negative pressure at the tail. It causes small refilling. In Fig.4-18, when expansion wave reflects at the thrust wall a refilling occurs at thruster wall.

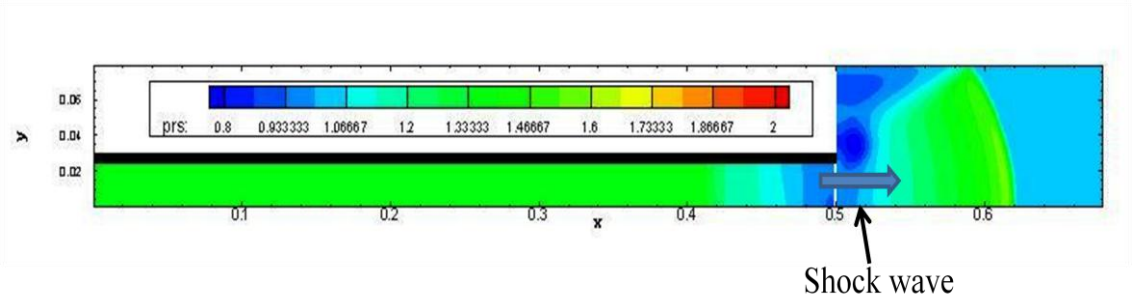

Figure 4-16 Calculated pressure contour at time =0.2504 ms. The shock wave is exhausted

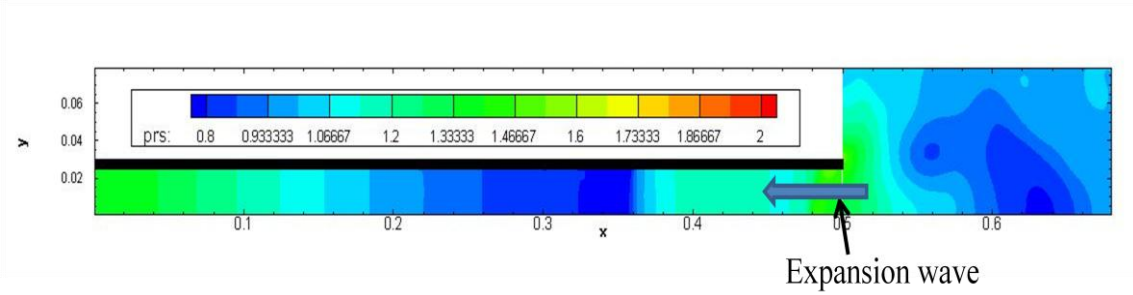

Figure 4-17 Calculated pressure contour at time =1.15 ms. The expansion wave propagates

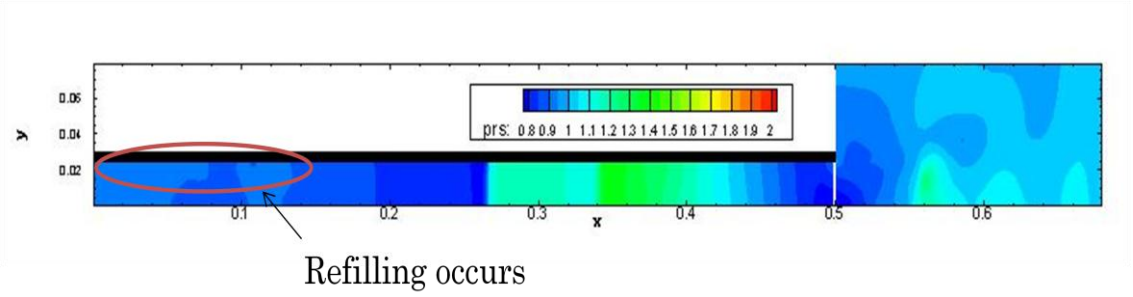

Figure 4-18 Calculated pressure contour at time =1.15 ms. Large refilling occur

4.6 Summary and Conclusion

A reed valve model was developed using CFD. Reed tip displacement responding to pressure difference was computed and mass flow through the reed valve was estimated by means of PFR. In addition, the pressure contour of reed valve and thruster were computed.

As a result, several barometers were obtained to develop reed valves. For instance, given design point as average pressure difference 0.1 atm ,reed length 20mm, width 10mm and reed tip displacement 2 mm, reed thickness should be 0.1mm. Additionally it is found that refilling from reed valve near open end is a little.

References of chapter 4

[1] J.Elson, “Gas pressure oscillations and ring valve simulation techniques for the discharge process of a reciprocating compressor”, *Ph.D. thesis, Purdue University*,1972

[2] J.P.Elson, W.sedel, ”Simulation of the Interaction of Compressor Valves with Acoustic Back Pressures in Long Discharge Lines” *Journal of Sound Vibration* **34**(2),pp211-220

[3] E.Pereira Parreira, J.R.Parise, “Performance Analysis of Capacity Control for Heat Pump Reciprocating Compressor”, *Heat Recovery System & CHP,* **13**(5),pp451-461

[4] Noriaki Ishii, Hiroshi Matsunaga, Michio Yamamura, Shigeru Muramatsu,Masafumi Fukushima, “Flow-Induced vibration of reed valve in Refrigerant Compressors”, *The Japan Society of Mechanical Engineer*s, 57(538),No90-1371B

[5] E. T. Hinds and G. P. Blair,”Unsteady Gas Flow Through Reed Valve Induction System”, *SAE Paper No780766*,1978

[6] G. P. Blair, E. T. Hinds, R. Fleck “Predicting the performance characteristics of two-cycle engines fitted with reed induction valves”,*SAE paper No 790842*,1979

[7] R. Fleck, G. P. Blair, R. A. R. Houston, An improved model for predicting reed valve 36ehavior in two-stroke cycle engines, *SAE Paper no. 871654*, 1987

[8] R. Fleck, A. Cartwrigth, D. Thornhill, Mathematical modeling of reed valve 36ehavior in high speed two-stroke engines, *SAE Paper no. 972738*, 1997

[9] Michele Battistoni, Carlo N. Grimaldi, Riccardo Baudille, Marcello Fiaccavento, Maurizio Marcacci,”Development of a Model for the Simulation of a Reed Vale Based Secondary Air Injection System for SI Engines”, *SAE Technical paper series, no.2005-01-0224*

[10] Wladyslaw Mitianiec, Andrzej Bogusz, “Theoretical and Experimental Study of Gas Flow Through Reed Valve in a Two-Stroke Engine”, *SAE Technical paper series, no.961802*,1996

[11] Dalibor Jajcevic, Raimund Almbauer,Stephan Schmidt, Karl Glinsner, Matthias Fitl, “Reed Valve CFD Simulation of a 2D Model Including the Complete Engine Geometry”, *SAE International no.2010-32-0015*,2010

[12] Anupam Dave, Asif Siddiqui, Daniel Probst Gregory J. Hampson, “Development of a Reed Valve Model for Engine Simulations for Two-Stroke Engines”, *SAE International no.2004-01-1455*, 2004

[13] R.Baudille, M. E. Biancolini, E. Mottola, “Optimization of dynamic reed valve behavior by material orientation”, *ASSOCIAZIONE ITALIANA PER L’ANALISI DELLE SOLLECITAZIONI XXXIV CONVEGNO NAZIONALE—14–17,*SETTEMBRE 2005

[14] G Cunningham, R J Kee, R G Kenny, “Reed valve modeling in a computational fluid dynamics simulation of the two-stroke engine”, *Proc. Instn. Mech. Engrs,*Vol 213 part D

[15] B. R. C. Mutyala, W. Soedel,” A Mathematical Model of Helmholtz Resonator Type Gas Oscillation Discharge of Two-Stroke Cycle Engine” *Journal of Sound and Vibration* **44**(4),pp479-491

[16] W. K. Anderson, J. L. Thomas, and B. V. Leer, “Comparison of Finite Volume Flux Vector Splitting for the Euler Equation”, *AIAA J.* **24**(9), 1986, 1453-1460

Chapter 5

Summary and Conclusion

5.1 One-dimensional Thruster Model

The model reproduced pressure oscillation of the inside thruster caused by the expansion wave and estimated mass flow through the reed valve. The predicted pressure wave dynamics shows good agreement with experimental results. The mass flow is assessed by PFR. As a result it was found that PFR start increasing when the expansion wave propagating from open-end, reaches thruster wall and increase of PFR by increase of α is saturated at around 0.08.

Comparing computations with experiments, α of the experiments was estimated at 0.006. The value is too small compare with that of preliminary prediction (around 0.04).

5.2 Reed valve model

One-dimensional model can represent tendency of pressure history and mass flow with low calculation cost. Reed valve motion was reproduced by spring-dumper model. In addition mass flow and reed tip displacement were investigated.

As a result, several barometers were obtained to develop reed valves. For instance, given design point as average pressure difference 0.1 atm ,reed length 20mm, width 10mm and reed tip displacement 2 mm, reed thickness should be 0.1mm. Additionally it is found that refilling from reed valve near open end is a little.

5.3 Conclusion

The pressure dynamics in the thruster was computed using one-dimensional computation. And the relationship of PFR and α was appeared.

Then in order to develop the reed valve system, the reed motion and inflow model were developed. As a result, several barometers were obtained to develop reed valves.

Acknowledgement

I would like to express my sincerest appreciation to Professor Kimiya Komurasaki in the University of Tokyo, who is the supervisor of this study and the chief referee of the thesis. He has given me a lot of opportunities not only to do study but also to make presentations in many conferences. He also gave me lots of structural advice and often asked me questions about the direction of my study. Therefore I could resolve many theoretical problems. I'm grateful to Professor Yoshihiro Arakawa (Department of Aeronautics and Astronautics) for his excellent advice and I've learnt attitude as a researcher or a student by his way.

I'm also grateful to Dr. Keishi Sakamoto (Plasma Heating Technology Group, Naka Fusion Institute, Japan Atomic Energy Agency) for giving our research groupe opportunities and ideas of experiments at JAEA. Gratitude is also extended to the following members in the group; Mr. Atsushi Kasugai, Dr. Koji Takahashi and Dr. Ken Kajiwara for cooperating experimental works and giving advice; Mr. Yukiharu Ikeda, Mr. Shinji Komori and Mr. Norio Narui for operating the gyrotron and helping my setups of our experiments; and Dr. Yukio Okazaki, Dr. Noriyuki Kobayashi and Mr. Kazuo Hayashi for giving special knowledge about each matter.

I thank elders and betters at our laboratory at the University of Tokyo, Dr. Yasuhisa Oda (JAEA), Dr. Makoto Matsui (Shizuoka Univ.), Dr. Shigeru Yokota, Mr. Bin Wang, Mr. Keigo Hatai, Mr. Yuya Shiraishi, Mr Toshikazu Yamaguchi, and Mr Kohei Shimamura for their fruitful discussions. Especially, Dr. Oda strongly supported my works at JAEA and let me know how to think against any matters. I also wish to thank all other members in Arakawa-Komurasaki-Koizumi laboratory.

学会誌掲載等

(1) 論文賞、学会賞などの受賞歴　1 件

1) **Poster award**：Masafumi Fukunari, Reiji Komatsu, Anthony Arnault, Toshikazu Yamaguchi, Kimiya Komurasaki, and Yoshihiro Arakawa, “Air-breathing Performance of Microwave Rocket with Reed Valve System”, *The 8th International Symposium on Applied Plasma Science* ,Sep.2011.

(2) 学術雑誌での発表論文及び著書　2件

2) Masafumi FUKUNARI, Toshikazu YAMAGUCHI, Reiji KOMATSU, Hiroshi KATSURAYAMA, Kimiya KOMURASAKI, Yoshihiro ARAKAWA, "Preliminary Study on Microwave Rocket Engine Cycle," *Plasma Application and Hybrid Functionally Materials*, Vol.20,p75, March 2011. **(査読有、掲載済)**

3) Masafumi Fukunari, Reiji Komatsu, Anthony Arnault, Toshikazu Yamaguchi, Kimiya Komurasaki and Yoshihiro Arakawa," Air-breathing of Microwave Rocket with Reed Valve System," *Vacuum* . **(査読有、修正稿審査中)**

(3) 国際会議等における発表

筆頭著者 3件

4) Masafumi FUKUNARI, Reiji KOMATSU, Toshikazu YAMAGUCHI, Kimiya KOMURASAKI, Yoshihiro ARAKAWA, Hiroshi KATSURAYAMA ,“Engine Cycle Analysis of Air Breathing Microwave Rocket with Reed Valves", *7th International Symposium on Beamed Energy Propulsion*, *BEAMED ENERGY PROPULSION: Seventh International Symposium. AIP Conference Proceedings*, Vol. 1402, pp. 447-456, Apr., 2011 **(査読有、掲載済).**

5) Masafumi FUKUNARI, Hiroshi KATSURAYAMA, Toshikazu YAMAGUTCHI, Kimiya KOMURASAKI, Yoshihiro ARAKAWA, “Analytical Study on Flight Performance of Microwave Rocket”、*The 28th International Symposium on Space Technology and Science*, 2011-q-11, June, 2011.

6) Masafumi Fukunari, Reiji Komatsu, Anthony Arnault, Toshikazu Yamaguchi, Kimiya Komurasaki, and Yoshihiro Arakawa, “Air-breathing Performance of Microwave Rocket with Reed Valve System,” The 8th International Symposium on Applied Plasma Science, Sep.,2011. Advances in Applied Plasma Science, Vol. 8, pp.105-106. **(上記Poster award)**

共著 1件

7) Yamaguchi T, Komatsu R, Fukunari M, Komurasaki K, Oda Y, Kajiwara K,

Takahashi K, Sakamoto K, "Millimeter-wave Driven Shock Wave for a Pulsed Detonation Microwave Rocket", *7th International Symposium on Beamed Energy Propulsion, Ludwigsburg*, *BEAMED ENERGY PROPULSION: Seventh International Symposium. AIP Conference Proceedings*, Vol. 1402, pp. 478-486 , Apr., 2011. **(査読有、掲載済)**

(4) 国内学会等における発表

筆頭著者　5件

8) 福成雅史、山口敏和、葛山浩、小紫公也、荒川義博、“マイクロ波ロケットによる低コスト打ち上げ手法の検討”、 第 13 回 SPS シンポジウム、東京、2010 年 10 月

9) 福成雅史、嶋村耕平、道上啓亮、葛山浩、小紫公也、荒川義博、“マイクロ波ロケット　による単段式打ち上げの検討”、第 54 回宇宙科学技術連合講演会、1P03、浜松、2010 年 11 月

10) 福成雅史、山口敏和、葛山浩、小紫公也、荒川義博、“パルスデトネーション型マイクロ波ロケットの非定常空気吸い込み過程の解析”, 航空原動機・宇宙推進講演会論文集、JSASS-2011-0019、広島、2011 年 3 月

11) 福成雅史、山口敏和、葛山浩、小紫公也、荒川義博、“パルスデトネーション型マイクロ波ロケットのリード弁をもちいた吸気機構の解析”、第４３回流体力学講演会／航空宇宙数値シミュレーション技術シンポジウム JSASS-2011-2021、東京、2011 年 7 月 **(査読済、JAXA-Special Publication として掲載予定)**

12) 福成雅史、Anthony Arnault、山口敏和、船木一幸、小紫公也、小泉宏之、荒川義博、“リードバルブによる吸気機構を取り付けたマイクロ波ロケットの飛行性能解析”、宇宙輸送シンポジウム、相模原 STEP-2011-028, 2012年1月

共著5件

13) 武市天聖, 山口敏和, 福成 雅史, 小紫公也, 小田靖久, 坂本慶司, "ミリ波駆動デトネーションの伝播速度制御によるマイクロ波ロケット推進 性能の向上", 第 55 回宇宙科学技術連合講演会、2K01, 松山, 2011 年 12 月

14) Anthony Arnault, 福成雅史, 小紫公也, 葛山浩, 荒川義博, "マイクロ波ロケットの軌道解析", 第 55 回宇宙科学技術連合講演会, 3E06, 松山, 2011 年 12 月

15) 小松怜史, 齋藤翔平, 福成雅史, 山口敏和, 小紫公也, 小田靖久, 梶原健, 高橋幸司, 坂本慶司, "マイクロ波ロケットにおけるリードバルブ式吸気機構の推力への影響", 平成 23 年度宇宙輸送シンポジウム, STCP-2011-078, 相模原, 2012 年 1 月

16) 嶋村耕平、福成雅史、道上啓亮、嶋田豊、柴田鉄平、小紫公也、荒川義博、“細い管内でのレーザー支持爆轟波の可視化と数値解析的考察”、平成23年度宇宙輸送シンポジウム, STCP-2011-027, 相模原, 2012年1月

17) 山口敏和、武市天聖、福成雅史、小紫公也、小田靖久、梶原健、高橋幸司、坂本慶司 ″

大気圧ミリ波プラズマの伝播速度制御とそのマイクロ波ロケットへの応用″, プラズマ・核融合学会 、23D02, 金沢, 2011 **(若手優秀発表賞)**